"POLITEHNICA" UNIVERSITY of BUCHAREST
APPLIED CHEMISTRY AND MATERIALS SCIENCE DOCTORAL SCHOOL

PhD THESIS SUMMARY

MULTIFUNCTIONAL NANOBIOMATERIALS

Author: MSc. Eng. Roxana Cristina Popescu

PhD Supervisor: Prof. Dr. Eng. Ecaterina Andronescu

PhD COMMITTEE

President	Prof. Dr. Eng. Adelina Ianculescu	from	"POLITEHNICA" University of Bucharest
PhD Supervisor	Prof. Dr. Eng. Ecaterina Andronescu	from	"POLITEHNICA" University of Bucharest
Reviewer	Prof. Dr. Mariana Carmen Chifiriuc	from	University of Bucharest
Reviewer	Conf. Dr. Eng. Alexandru Mihai Grumezescu	from	"POLITEHNICA" University of Bucharest
Reviewer	Ist degree Sci. Res. Dr. Mihai Radu	from	National Institute for Research and Development in Physics and Nuclear Engineering "Horia Hulubei"

BUCHAREST
2020

Table of Contents

List of notations

NP	nanoparticles
Fe_3O_4	magnetite
FDA	Food and Drug Administration
PEG	polyethylene glycol
@	core-shell
RMN	nuclear magnetic resonance imaging
CT	computer tomograph
ADN	dezoxiribonucleic acid
GEM	gemcitabine
DOX	doxorubicine
SAED	selected area electron diffraction
TEM	transmission electron microscopy
TGA	thermogravimetric analysis
EDX	energy dispersive X-Ray spectroscopy
SEM	scanning electron micrscopy
PIXE	particle-induced X-Ray emission
XRD	X-Ray diffraction
MTT	3-(4,5-dimethylthiazol-2-yl)-2,5- diphenyltetrazolium bromide
MTS	3-(4,5-dimethylthiazol-2-yl)-5-(3-carboxymethoxyphenyl)-2-(4-sulfophenyl)-2H-tetrazolium
PI	propidium iodide
BrdU	bromodeoxyuridine
γ- H2AX	phosphorylated histonic protein X from H2A family
PBS	Phosphate Buffer Saline
DMF	dose modifying factor
JCPDS	Joint Committee on Powder Diffraction Standards
MEM	Minimum Essential Medium Eagle
DMEM	Dulbecco's Modified Eagle's Medium
FBS	Fetal Bovine Serum
Pimo	Pimonidazole
2D	bi-dimensional
3D	tri-dimensional

Key words: *magnetite nanoparticles, anti-tumor, chemosensitization, radiosensitization.*

Acknowledgement

For the elaboration of the PhD Thesis entitled "Multifunctional Nanobiomaterials" I benefited from the collaboration with several exceptional researchers whom I would like to recognize. The presented experiments were done at "Politehnica" University of Bucharest (PUB), in collaboration with "Horia Hulubei" National Institute for Physics and Nuclear Engineering (NIPNE), Medical Faculty of Mannheim of Heidelberg University (UMM) and Medical University of Vienna (MUW).

First of all, I would like to thank Prof. Ecaterina Andronescu for the supervision of my research activity in the preparation of my PhD Thesis, but also to the scrientific advisers Dr. Denisa Ficai, Dr. Bogdan Ștefan Vasile and Dr. Alexandru Mihai Grumezescu (PUB). Also, I would like to especially acknowledge my colleagues from NIPNE, Dr. Diana Iulia Savu, Dr. Mihaela Temelie, Dr. Mihai Radu and Dr. Ioan Dorobanțu, as well as Prof. Anton Ficai from PUB, to whom I thank for guidance and support.

Thank you to the PhD evaluation committee: president Prof. Adelina Ianculescu and reviewers Prof. Mariana Carmen Chifiriuc, Dr. Alexandru Mihai Grumezescu and Dr. Mihai Radu.

I would like to thank Prof. Marlon R. Veldwijk, Dr. Carsten Herskind (UMM), Prof. Wolfgang Doerr and Dr. Verena Kopatz (MUW) for guidance and support in performing he radio-sensitization studies involving nanoparticles.

Not at last, I would like to thank the following collaborators for facilitating the help and access facility in performing several physico-chemical analysis: Prof. Georgeta Voicu, Ing. Roxana Trușcă, Dr. Bogdan Ștefan Vasile (PUB), Dr. Mihai Straticiuc, Dr. Dragoș Mirea, Ing. Radu-Florin Andrei (NIPNE), Dr. Adina Boldeiu (Microtechnologies Institute Bucharest), Tehn. Hiltraud Hosser (UMM). I would like to thank Dr. Irina Păun, Dr. Cătălin Luculescu, Ing. Oana Gherasim și Dr. Gabriel Socol (National Institute for Laser, Plasma and Radiation Physics) for the collaboration.

I am grateful to my family for the moral support and understanding regarding my research activity.

For the financing of the experiments presented in this thesis, I would like to acknowledge the Romanian Ministry of Education and Research (grants no. PN18090202/2018 and PN19060203/2019), the German Academic Exchange Service - Deutscher Akademischer Austauschdienst (DAAD) (grant no. 57299291), Austrian Federal Ministry of Education, Science and Research - Bundesministerium für Bildung, Wissenschaft und Forschung, through the Austrian Agency for International Cooperation in Education - OeAD (grant no. ICM-2018-10056) and the Romanian Ministry of European Funds (Operational Programme Human Capital – financial agreement 51668/ 09.07.2019, SMIS code 124705).

The Author

I. Critical literature study

Lately, magnetite (Fe_3O_4) nanoparticles (NP) have gained attention especially in medical applications oriented towards clinical implementation, many of them already being approved for clinical use by Food and Drug Administration (FDA) in diagnosis [1], hyperthermia cancer treatment [2] or combating iron (Fe) deficiencies [3]. This was possible due to its properties like biocompatibility [4], biodegradability [5], magnetic properties [6] and use in functionalization [7]. Besides its advantageous properties, magnetite nanoparticles have some major flaws, given by their rapid aggregation, chemical reactivity, high surface energy and oxidation, which can alter their biocompatibility, properties or performances. To prevent these unwanted events, different functionalization methods have been applied [8].

Tremendous effort has been made in the attempt to functionalize magnetite nanoparticles. Among these, the conjugation of magnetite nanoparticles using polymers can be done through both *in situ* and post-symthesis methods. It is often encountered in case of co-precipitation synthesis of Fe_3O_4 nanoparticles to introduce polymer molecules in the precipitation solution, in order to simultaneously determine the nucleation, growth and functionalization of the NP [9, 10]. In this case, non-covalent bonds (electrostatic interactions) are formed between polymers and magnetite nanoparticles. This method is preffered in case of drug delivery applications. On the other hand, the post-synthesis functionalization method starts from previously synthesized magnetite nanoparticles, which can be conjugated with different polymers through the hydroxyl chemical groups available on the NP surface. Most of the time, these are condensation reactions, such as the formation of ester bonds.

During the development of biomedical applications based on Fe_3O_4 nanoparticles it is important to prove the functionality of the proposed system. This can be initially done for simple biological models, which simulate certain properties in the human body. Generally, this evaluation process starts with *in vitro* testing, which is done in controlled medium, on different cell cultures, relevant for the study. Conventionally, these are 2D cell cultures, which are excellent models for mechanistic studies of cellular and molecular biology, of cells physiology and biochemistry, testing of drugs and toxic compounds effects, respectively for mutagenesis and carcinogenesis. *In vitro* 3D models have some major advantages compared to 2D models, given by a similar organization of tumor cells within *in vivo* models. Thus, the proteic and genic expression, the protein gradient, cell signaling, cell migration and response to treatment are similar as in case of *in vivo* conditions.

A potential approach in the improvement of cancer treatment efficiency is the use of nanotechnology. The advantage of using nanoparticles is given by their ability to target the desired area (such as the tumor area) once they are introduced in the systemic circulation. This can be done not just through passive transport (simiar as in case of most clinically available pharmaceutic substances), but a specific active transport can also be implemented. Passive transport is reffering to the enhanced permeability and retention effect at the tumor site, which is explained by the defects in the blood vessels architecture in the tumor area, but also by the weak lymphatic drenaige. On the other hand, the active transport can be either obtained through magnetic guiding, either through the application of different functionalization agents, which can ensure the nanoparticles specificity to the receptors on the surface of the targeted cells.

The conjugation of magnetite nanoparticles with other compounds can improve their multi-functionality and implementation of properties, such as enhanced and/or specific internalization in cancer cells [11, 12], but can also help in the modulation of the active substance delivery profile through different mechanisms: (1) drug protection, (2) delivery delay or (3) triggered drug delivery (mediated by pH, temperature, light, biological enzimes, etc.). In this regards, polyethylene glycol (PEG) was extensively used in pharmacological applications due to properties like: (1) high solubility in aqueous media; (2) minimization of the

opsonization phenomenon; (3) spacer function for different molecules and targeting agents, which minimize non-specific interactions.

Cancer therapy using radiation is based on deliverying a high dose at the tumor site, in order to maximally inhibit the growth of tumor cells, while in the same time trying to protect the surrounding healthy cells. The radiosensitizers based on high atomic number elements have the property to absorb most of the incident radiation, compared to the surrounding tissue and, due to photoelectric and Compton effects, to deliver low energy photons, Auger secondary electrons and low energy secondary electrons. This secondary radiation enhances the production of reactive oxygen species, but in case of nanoparticles, the interaction and intercalation in the DNA is favored [13]. The biological effects of nanoparticles radiosensitization imply the alteration of cellular signaling pathways involved in: (1) oxidative stress, (2) cell cycle disruption and respectively (3) DNA repair inhibition [14].

Despite the increased interest in the utilization of nanoparticles as drug delivery systems and radiosensitizers, the clinical implementation has not been yet done [15]. One of the shorcomings which prevent the clinical translation of these applications is given by the non-specific targeting. Another problem is given by the inability of nanoparticles to be intracellularly retained following the penetration of the bilipidic layer and their passage into the cytoplasmatic compartments.

II. Original contributions

Justification of subject choice

Cancer is a complex series of pathological conditions, determined by the consistent damage of a tissue or by host- environment interactions. Worldwide, in 2017, cancer was the second cause of death after cardiovascular diseases [16, 17]. 80000 new cancer cases were recorded in Romania in 2018 [18]. In this context, one of the main concerns regarding biomedical research is the development of a new method for cancer treatment, which can bring an improved response in reducing the adverse effects and improving the patient comfort.

The **main purpose** of the project was to construct and evaluate multifunctional nano-systems based on magnetite nanoparticles for the delivery of active substances (chemotherapeutics) in order to modulate the chemical and radiological response of tumor cells.

Specific objectives:

(1) Obtaining and physico-chemical characterizing of magnetite carriers; selecting and optimizing the systems;
(2) Obtaining an *in vitro* anti-tumor effect of magnetite nanoparticles specific for a certain tumor cell line;
(3) Obtaining an *in vitro* anti-tumor effect of magnetite nanoparticles in 3D cell models;
(4) Measuring the internalization efficiency of magnetite nanoparticles in the presence or absence of ionizing radiation;
(5) Mechanistic characterization of magnetite nanoparticles internalization efficiency in the presence or absence of ionizing radiation;
(6) Obtaining an *in vitro* anti-tumor effect of magnetite nanoparticles in the presence or absence of ionizing radiation;
(7) Mechanistic characterization of magnetite nanoparticles influence on the state of tumor cells (cell cycle phase or cell death) in the presence or absence of ionizing radiation.

Contributions regarding the Fe_3O_4 nanoparticles design, synthesis and characterization

For the synthesis of the Fe_3O_4 nanoparticles used in this study, the co-precipitation method was applied [19], due to the advantages it provides, such as reproducibility, high yield synthesis, ease and reduced costs. In order to functionalize these nanoparticles, both *in situ* and post-synthesis methods have been employed. Also, the anti-tumor drug was introduced in the nano-system through: (1) direct conjugation with the end functional groups of magnetite, by using both *in situ* and post-synthesis approaches and also through (2) encapsulation in a polymeric shell.

In situ gemcitabine functionalized nanoparticles

The characterization of crystallinity degree and identification of the resulted samples was done using the X-Ray diffraction (XRD) (Fig. II.1) and selectected area electron diffraction (SAED) (Fig. II.3.C). The diffraction interferences of magnetite were indexed using the JCPDS no. 19-0629 standard. The presence of the organic chemotherapeutic substance did not affect the crystallinity of the nanoparticles and did not induce other significant changes in the phase composition of the samples.

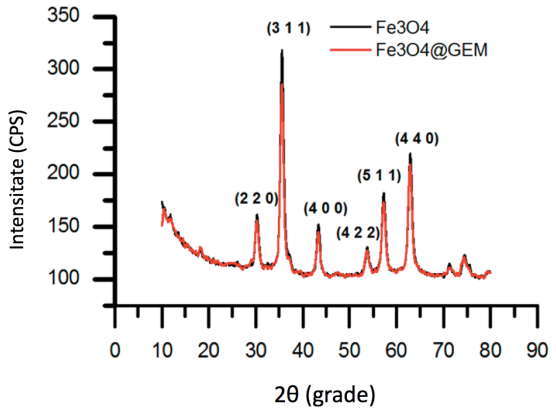

Fig. II.1. X-Ray diffraction spectrum for Fe_3O_4 and Fe_3O_4@GEM; [20]

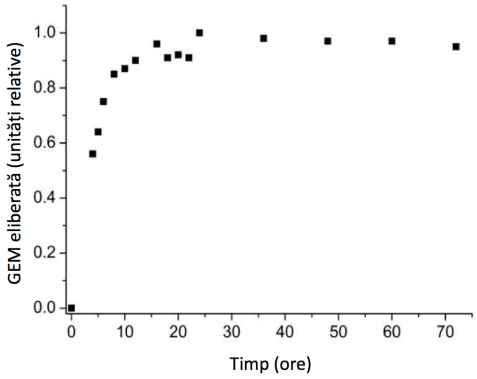

Fig.II.2. Gembitabine drug delivery kinetics from Fe_3O_4@GEM; [20]

The thermogravimetric analysis was used to measure the gemcitabine quantity, which interacts with magnetite nanoparticles, based on the mass difference resulting following the thermal treatment applied to Fe_3O_4@GEM. Thus, a reduction with 6,8% resulted following the degradation of GEM.

Transmission electron microscopy (TEM) (Fig. II.3) gave more information regarding the (non-)functionalized nanoparticles crystallinity. From the high resolution TEM images (Fig. II.3. B), a high degree of crystallinity was observed for both samples. In case of Fe_3O_4@GEM, GEM individually covered each nanoparticle, resulting in an amorphousa and continous coating at the surface of Fe_3O_4 nanoparticles, forming core-shell structures. Fig. II.3.B emphasizes the (220) crustalline plane of 0,29 nm, which is characteristic for the mineralogical phase magnetite [21].

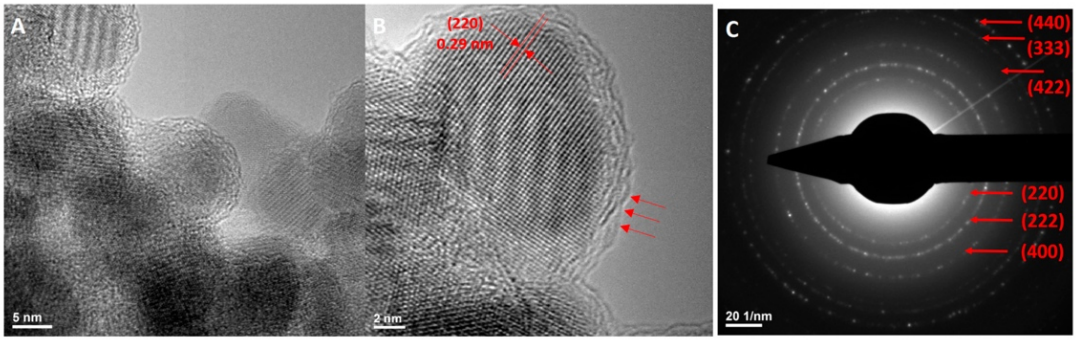

Fig. II.3. (A) TEM, (B) HRTEM and (C) SAED spectrum for Fe_3O_4@GEM. [20]

The behavior of GEM functionalized Fe_3O_4 nanoparticles in two different cell culture mediums (DMEM and MEM) was evaluated, by investigating the nanoparticles stability and their hydrodynamic diameters for a dilution interval of 0,25 to 0,025%. The colloidal stability of the stock solutions (1% nanoparticles in deionized water) was emphasized: Zeta potential of -32,69 mV, mean hydrodynamic diameter of 176,9(±15) nm. The hydrodynamic diameters of Fe_3O_4@GEM in complete DMEM were comprised between the range of 218-280 nm, while the Zeta potential was between -12 and -23 mV for the investigated nanoparticle concentration range. Fe_3O_4@GEM in complete MEM had values of the Zeta potential above 20 mV and proved an increased stability, compared to the suspensions in DMEM, while the hydrodynamic diameters were in the range of 238 and 270 nm. The polydispersity indices were less than 0,3, which is an indicator for monodisperse systems [22]. GEM functionalized magnetite nanoparticles proved that the delivery of the drug in the surrounding media took place in the first 24h, potentially assuring a longer presence of the drug in the blood flow.

In situ doxorubicin functionalized nanoparticles

X-Ray diffraction spectrum was characteristic for the mineralogical phase magnetite (JCPDS standard no. 19-0629 [23]), no secondary phases being detected. Also, the introduction of doxorubicin in the reaction system did not affect the composition nor the crystallinity of the samples. The drug quantity interacting with the iron oxide nanoparticles was determined through thermogravimetric analysis and was 0,415% DOX.

The TEM and HR-TEM investigations evidenced the presence of doxorubicin in the conjugated nanoparticles, which formed a low crystalline mass around the highly crystalline aggregates (Fig. II.4. B), leading to the formation of core-shell structures. The high degree of crystallinity (Fig. II.4. C) was confirmed through the selected area electron diffraction method. The SAED spectrums confirmed the XRD spectrums. The X-Ray diffraction analysis, HR-TEM and SAED proved that the presence of DOX in the reaction medium did not alter the crystallinity nor the composition of the resulted compound.

The behavior of Fe_3O_4@DOX in the biological media was studied by measuring the Zeta potential and the hydrodynamic diameter of the constructs, in complete MEM culture medium and standard conditions of temperature and humidity. The resulted conjugated magnetite nanoparticles proved to be highly stable (Zeta potential of -36,79 mV) and had hydrodynamic diameters of 108,3 nm. The Fe_3O_4@DOX dillutions in culture medium (500, 100, respectively 10 μg/mL) proved a good stability of the negatively charged nano-constructs (zeta potential of -26,67 mV for the highest concentration in the study).

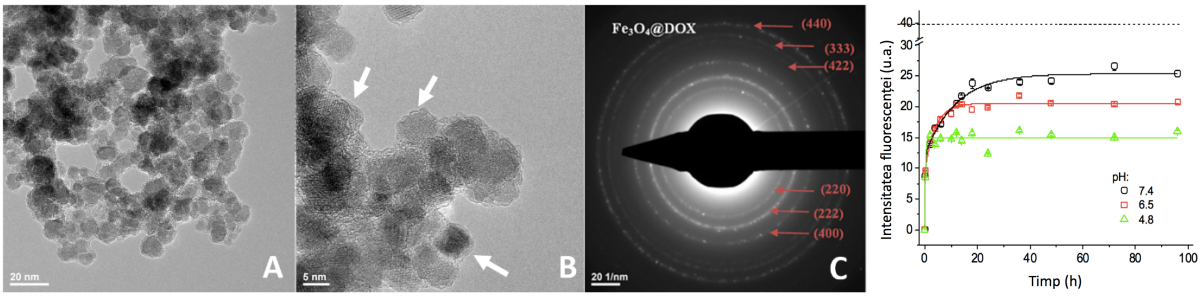

Fig.II.4. TEM, HR-TEM and SAED for Fe_3O_4@DOX (A-C). (D) DOX delivery kinetics from Fe_3O_4@DOX in biological media with different pH; data is shown as mean±SEM; the dotted line represents the fluorescence intensity measured in a DOX solution in equivalent concentration to Fe_3O_4@DOX; figure adapted from [24];

The delivery kinetics study of DOX in mediums with different biologically relevant pH values revealed that the active substance is gradually released in PBS until 72h of incubation, with an exponential delivery during the first 16h (Fig. II.4. D). Results proved the drug was released in an inversely proportional manner compared to the pH of the delivery medium.

Post-synthesis doxorubicin functionalized nanoparticles

Specrophotometrical measurements were done for the rest of the aqueous medium in which the loading of DOX in Fe_3O_4 nanoparticles took place. The results proved that an insignificant quantity of DOX interacted with the Fe_3O_4 nanoparticles, at 24 and 48h of reaction. Moreover, these observations were confirmed by fluorescence measurements.

***In situ* polyethylene glycol functionalized nanoparticles**

X-Ray diffraction was used to identify the diffraction interferences for magnetite (JCPDS standard no. 19-0629), as well as the high crystallinity degree of nanoparticles. These observations were confirmed through SAED spectrums and HR-TEM microscopy (Fig. II.5-II.8. c-d). Transmission electron microscopy was used to evaluate the morphology of the magnetite nanoparticles functionalized with polyethylene glycol with different molecular weights. Thus, Fe_3O_4-PEG 4K, 6K, respectively 20K nanoparticles showed a spherical morphology (Fig. II.5, II.6, II.7), having diameters of: 11,028±2,447 nm for Fe_3O_4- PEG 4K, 12,33±2,748 for Fe_3O_4- PEG 6K, respectively 12,932±4,023 nm for Fe_3O_4- PEG 20K. By increasing the polymer molecular weight to 35K, the nanoparticles morphology was strongly affected, their dimension increasing (17,523±10,55) and having a rhombic shape (Fig. II.8). Additionally, the presence of some spherical nanoparticles with small dimensions was noticed. This was probably caused by an incomplete functionalization.

DOX loading efficiency in the resulted nanoparticles was determined through spectrophotometrical measurements. The NP proved an effect which was dependent on the polymer molecular weight and the loading time. A significant effect was observed in case of Fe_3O_4-PEG 6K, which proved a drug loading efficiency of 24,48% at 24h, respectively 40,95% at 48h [25].

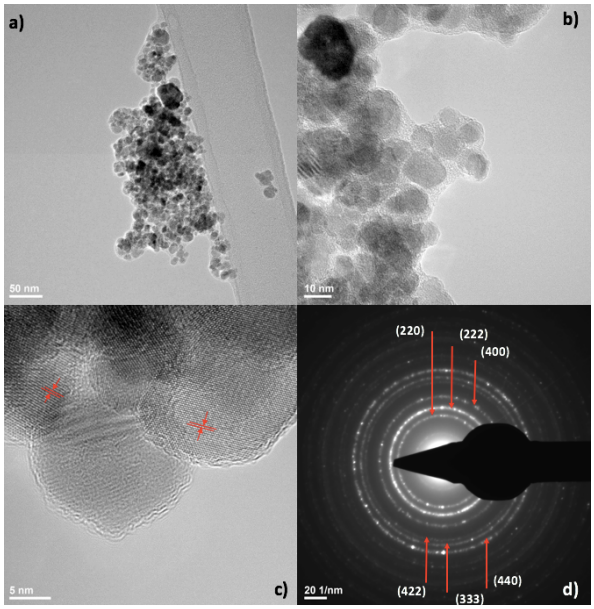

Fig. II.5. TEM (a,b), HR-TEM (c), respectively SAED (d) for Fe_3O_4- PEG 4K;

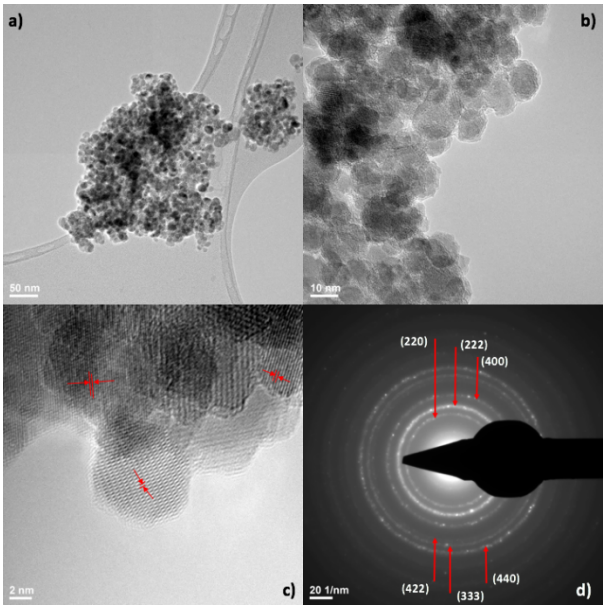

Fig. II.6. TEM (a,b), HR-TEM (c), respectively SAED (d) for Fe_3O_4- PEG 6K; [25]

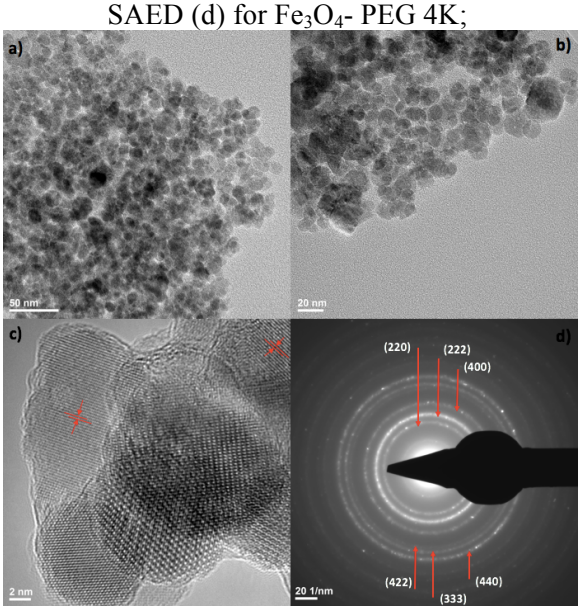

Fig. II.7. TEM (a,b), HR-TEM (c), respectively SAED (d) for Fe_3O_4- PEG 20K;

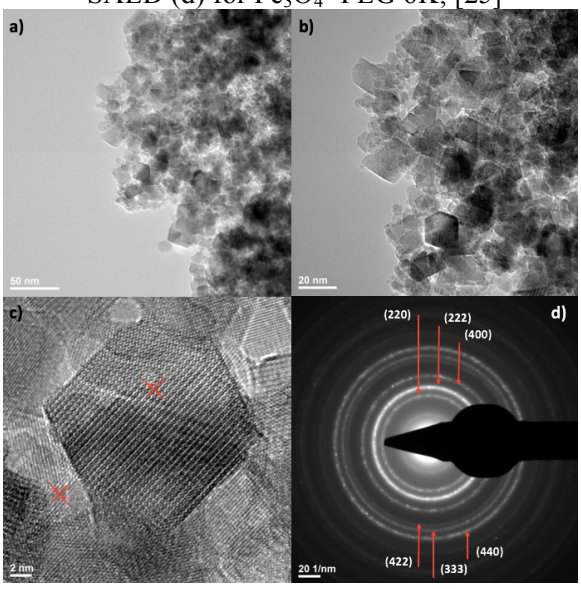

Fig. II.8. TEM (a,b), HR-TEM (c), respectively SAED (d) for Fe_3O_4- PEG 35K;

Post-synthesis polyethylene glycol functionalized nanoparticles

The obtaining of Fe_3O_4@PEG 6K/ DOX was done using a three step synthesis method, resulting in the obtaining of highly crystalline nanoparticles (Fig. II.9. A-C); these showed diffreaction rings characteristic to the spinel structured face centred cubic magnetite mineralogical phase (Fig. II.9. D). HR-TEM confirmed the data on the crystallinity of the nanoparticles and emphasized the presence of (220) crystalline plane with 0,29 nm witdth (Fig. II.9. D), characteristic for the magnetite mineralogical phase. The post-synthesis functionalization of iron oxide nanoparticles with polyethylene glycol determined the individual coverage of the NP with an organic phase with reduced crystallinity, forming core-shell structures, as emphasized by the HE-TEM images (Fig. II.9. A-C, PEG layer is emphasized with white arrows). The DOX loading efficiency in Fe_3O_4@PEG 6K/ DOX was 1,11%.

The measured mean hydrodynamic diameter was 164,2 nm and the Zeta potential measurements showed a good stability (14,8 mV for stock solutions, with no prior ultrasound treatment). Nevertheless, the loading of DOX determined an increase in the hydrodynamic diameter and a modification of the surface charge towards negative values. Both of the constructs were monodisperse systems. The delivery experiments were done in three mediums with different values of pH, the Fe_3O_4@PEG6K/ DOX nanoparticles proving a rapid initial delivery which was independent of the pH of the medium (Fig. II.10).

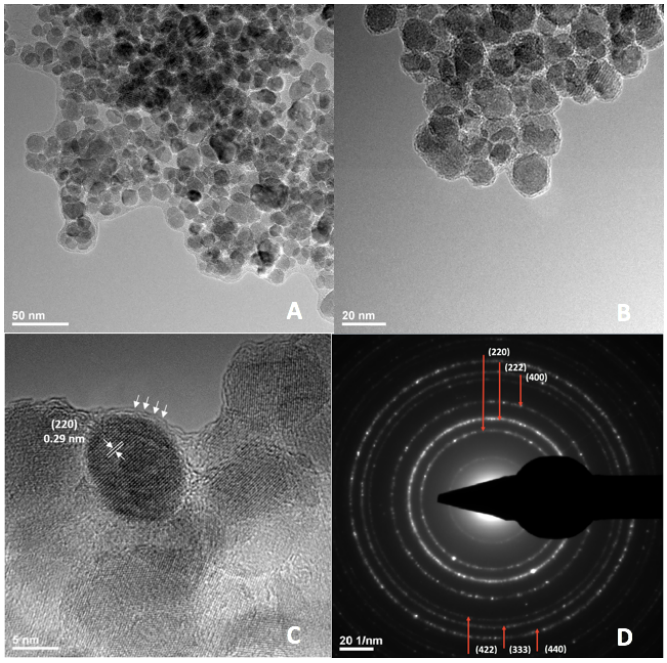

Fig. II.9. Structural and compositional characterization of Fe_3O_4@PEG 6K: (A) TEM, measure bar 50 nm; (B) TEM, measure bar 20 nm; (C) HR-TEM, measure bar 5 nm; (D) SAED spectrum; [26]

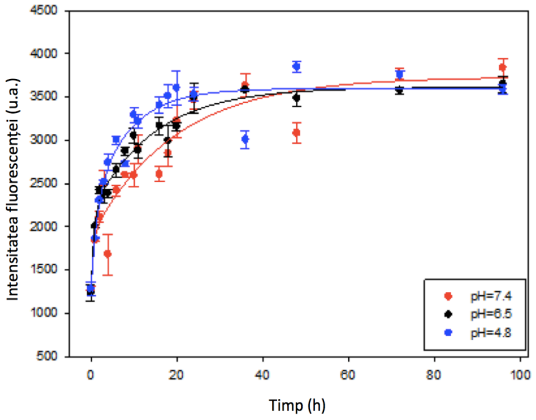

Fig. II.10. DOX delivery from Fe_3O_4@PEG6K/ DOX constructs at 37°C (0-96h); [26]

Nanoparticles selection for biological studies

In order to select from the previously synthesized nanoparticles for further biological chemo- and/or radio-sensitization studies of cancer cells, a series of parameters have been taken into consideration.

The study initially started with two anti-tumor drugs, namely gemcitabine and doxorubicine. DOX was chosen as model active substance in the following biological studies due to its applicability in the treatment of numerous cancers and its native fluorescence property, which facilitates the visualization of the conjugated/ loaded nanoparticles.

Concerning the *in situ* PEG functionalized magnetite nanoparticles, the NP characterization studies revealed a variability in morphology and non-homogenity. The best *in vitro* biological behavior was obtained for Fe_3O_4-PEG 6K, which induced values of the cells viability above 80% after 48h of interaction. Regarding the functionalization method, the post-synthesis method was preferred, because it resulted in the obtaining of core-shell nanoparticles, the total quantity of loaded DOX after 24h being 1,11 wt% [26], while Fe_3O_4-PEG 6K/DOX (*in situ* functionalized) had a quantity of 0,49 wt% DOX [25].

II.3. Contributions regarding the evaluation of Fe_3O_4 nanoparticles chemosensitization potential

II.3.1. Biological mechanisms evaluation of Fe_3O_4 nanoparticles directly conjugated with active substances

II.3.1.1. *In situ* gemcitabine functionalized Fe_3O_4 nanoparticles

The cytotoxicity of GEM functionalized nanoparticles (Fe_3O_4@GEM) was evaluated for three human tumor models: BT474 human mammary gland ductal carcinoma (Fig. II.12), HepG2 human hepatocellular carcinoma (Fig. II.13) and MG-63 human osteosarcoma (Fig. II.14). For the characterization of these effects, it was used an *in vitro* test which measures the cell viability and is based on tetrazolium salts. The cytotoxic effect of Fe_3O_4@GEM on tumor cells was characterized by comparison with magnetite and free GEM, in equivalent concentrations, for 3 time intervals (24, 48 and respectively 72h). The free GEM concentrations were calculated from the TGA measurements (capiter II.2.3.2. *In situ* gemcitabine functionalized nanoparticles).

For all three cell lines, the unfunctionalized magnetite nanoparticles did not show significant changes regarding the viability at none of the investigated time intervals (Fig. II.12-II.14, black squares graphs). Magnetite nanoparticles proved to be biocompatible, as the viability values were above 80%, according to ISO 10993-12:2001(E).

Concerning the effect of Fe_3O_4@GEM on the BT474 cell line (Fig. II.12), results proved a cytotoxic potential (viability of 60%, compared to control), starting from 24h of treatment, for the highest equivalent concentration. The anti-tumor effect was more pronounced with time, at 48 and 72h after treatment. The drug activity, free or conjugated with nanoparticles was dependent on time and the administered dose. A potentiating effect of the nanoconjugate, compared to free GEM was observed for the highest concentration (0,15 mg/mL GEM equivalent concentration) at all time intervals (Fig. II.12).

For HepG2 cells (Fig. II.13), at 24 and 48 h after the tratament, the cell viability following free GEM and Fe_3O_4@GEM administration decreased down to about 80%, compared to control, independently of concentration. For the highest equivalent GEM concentration (0,15 mg/mL), the effect determined by the nano-conjugate was significantly higher than free GEM, the cytotoxic effects being accelerated until 72h after the treatment. At this time interval, the viability decreased with 40% in case of Fe_3O_4@GEM, compared to the free drug, for the highest equivalent concentration employed in the study (Fig. II.13. C).

MG6-3 human osteosarcoma cell line is gap jonctions positive. Free GEM proved to be strongly cytotoxic for this type of cells, starting with the lowest concentrations employed in the study (Fig. II.14). Free GEM cytotoxic activity was more pronounced than the effect induced by the nano-conjugate. Nevertheless, Fe_3O_4@GEM proved to be highly cytotoxic for the highest equivalent concentration of GEM (0,12 mg/mL), determining a viability below 40%, at 72 h of treatment.

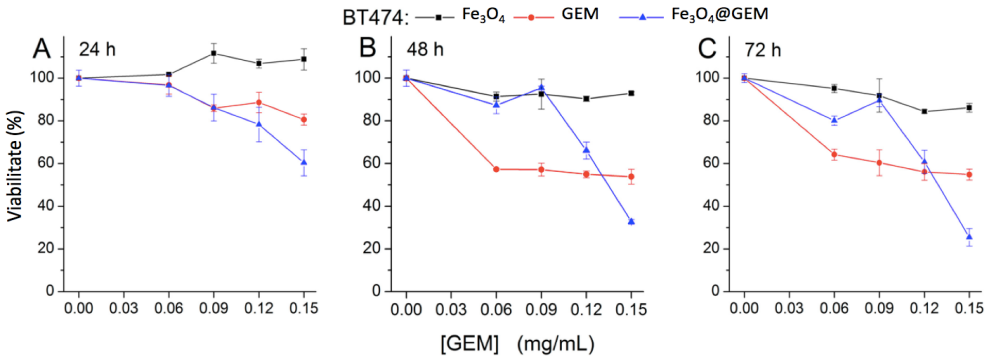

Fig. II.12. Cell viability for BT474, incubated with free GEM, Fe_3O_4@GEM and Fe_3O_4 (equivalent GEM concentrations), determined at (A) 24h; (B) 48h and (C) 72h after the tratament. Results are percent of untreated control [20].

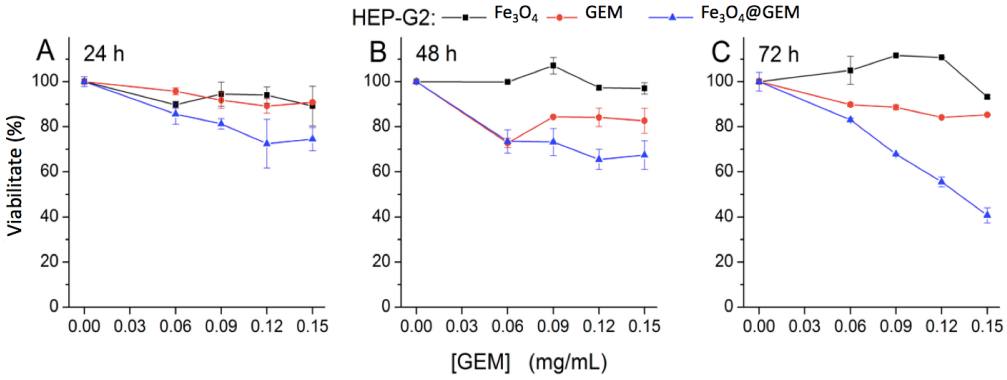

Fig. II.13. Cell viability for HepG2, incubated with free GEM, Fe_3O_4@GEM and Fe_3O_4 (equivalent GEM concentrations), determined at (A) 24h; (B) 48h and (C) 72h after the tratament. Results are percent of untreated control [20].

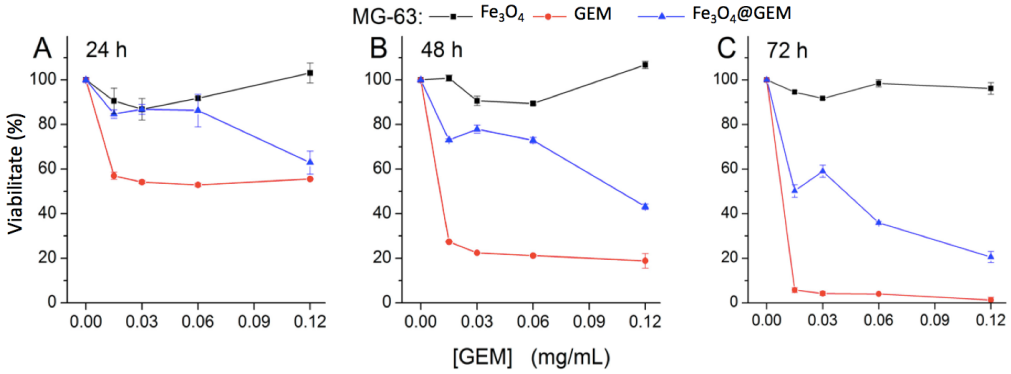

Fig. II.14. Cell viability for MG-63, incubated with free GEM, Fe_3O_4@GEM and Fe_3O_4 (equivalent GEM concentrations), determined at (A) 24h; (B) 48h and (C) 72h after the tratament. Results are percent of untreated control [20].

It is known that free GEM is internalized in cells through nucleoside transporters [27], while inorganic nanoparticles can be internalized either through endocytosis, either by direct diffusion in the cells [28]. The specific interaction between nanoparticles and the kinetics of these processes can explain the differences in the cytotoxic response of each cell line.

For further investigations of the Fe_3O_4@GEM toxic effects, alterations in the cells morphology were investigated. Scanning electron microscopy and energy dispersive X-Ray spectroscopy were used to evaluate the localization of the nano-structured systems following their interaction with tumor cells during 24h. In case of BT474 cells (Fig. II.15), the morphological scattered electron images (Fig. II.15. B) proved the presence of nanoparticle aggregates at the exterior of cells (emphasized with red circles). This analysis showcases the elements with higher atomic number with lighter grey levels (such as Fe), while the elements

with lower atomic number (such as C) are represented with darker grey levels. The yellow square (Fig. II.15. B) marks an area which is free of high atomic number elements, thus there are no extracellular Fe nanoparticles (in comparison to the morphological image resulted from the signal reveived from secondary electrons- Fig. II.15. A). This area was subjected to EDX mapping. Similarly as in Fig. II.15. B, in Fig. II.15. D, extracellular Fe_3O_4@GEM aggregates are evidenced, which are marked with red squares (green colored dots with high luminous intensity). The yellow square emphasizes the presence of Fe aggregates, which correspond to the area in Fig. II.15. B, where Fe nanoparticles are not noticeable in the exterior of the cells. These Fe aggregates are covered by an organic layer (Fig. II.15. B). Moreover, this area marked with the yellow square was subjected to EDX quantitative analysis, the elemental atomic composition showing a concentration of 0,33 %at Fe, with an error of 18,47%.

A similar behavior could be evidenced in case of HepG2 (Fig. II.16). Here, the EDX quantitative evaluation was done for two areas clearly distinguished by the localization of the nanoparticles: area 1 which presents ligh grey nanoparticle aggregates, situated in the exterior of the cell membrane and area 2 which represented in a darker grey level, free of high atomic number elements (Fig. II.16. D). The results for the quantitative measurements showed a concentration of 0,25%at Fe, with an error of 23,09% for area 1, respectively 0,06%at Fe, with an error of 62,01% for area 2.

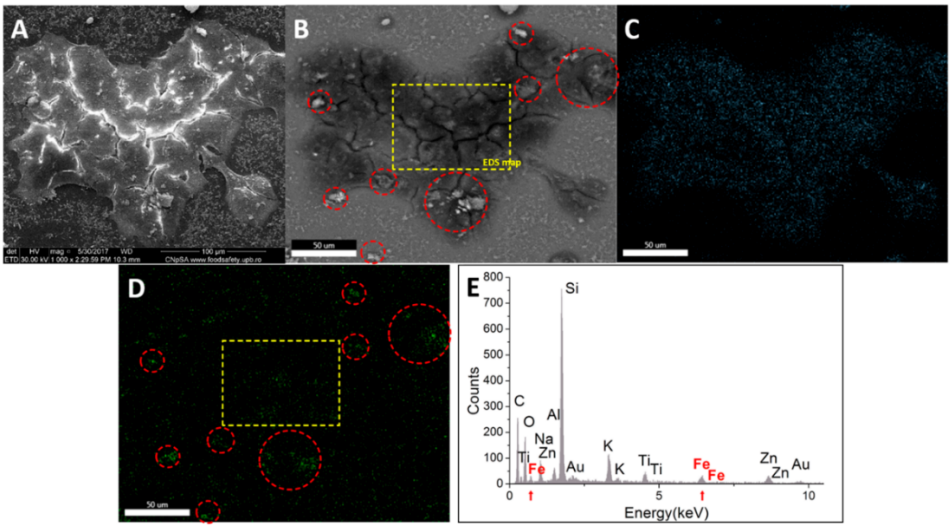

Fig. II. 15. Qualitative and quantitative elemental characterization of BT474 cells exposed to the highest concentration of Fe_3O_4@GEM during 24 h: (A) morphological image resulted using the signal resulted from secondary electrons (magnification 1000x); (B) morphological image resulted using the signal resulted from scattered electrons (magnification 1000x); (C) elemental mapping for C atoms in image B; (D) elemental mapping for Fe atoms in image B; (E) EDX spectrum for image B (yellow square); the red cicles mark areas with extracellular nanoparticle aggregates; the yellow square marks an area free of extracellular nanoparticle aggregates, which was subjected to quantitative elemental analysis; the red arrows mark the presence of Fe in the area for which EDX analysis was done [20].

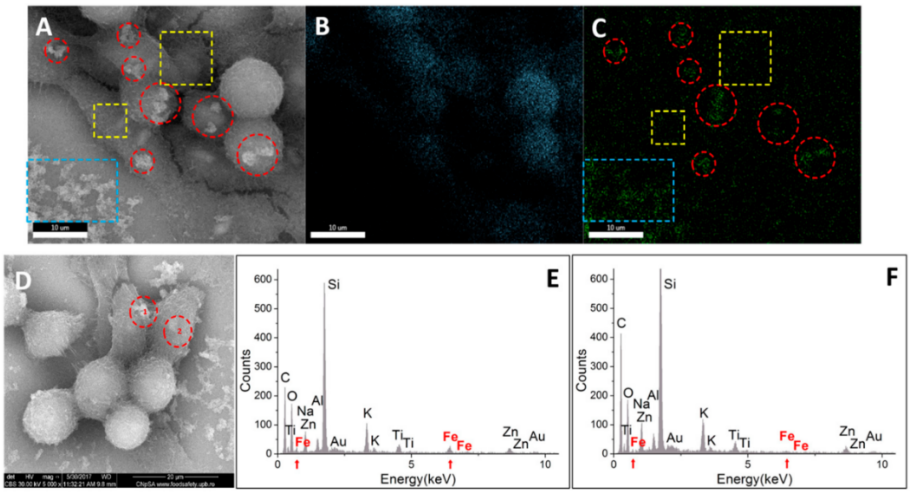

Fig. II.16. Qualitative and quantitative elemental characterization of HepG2 cells exposed to the highest concentration of Fe_3O_4@GEM during 24 h: (A) morphological image resulted using the signal resulted from secondary electrons (magnification 10000x); (B) elemental mapping for C atoms in image A; (C) elemental mapping for Fe atoms in image A; (D) morphological image resulted using the signal resulted from scattered electrons (magnification 5000x); 1- area with nanoparticle aggregates situated in the exterior of the cell membrane; 2- area free of elements with high atomic number; (E) EDX spectrum for image D (area 1); (F) EDX spectrum for image D pentru imaginea D (area 2); red circles mark areas with extracellular nanoparticle aggregates; the yellow square marks an area free of extracellular nanoparticle aggregates; the blue square marks an area where nanoparticles were attached to the glass substrate; red arrows mark the presence of Fe in the area where EDX analysis was done [20]

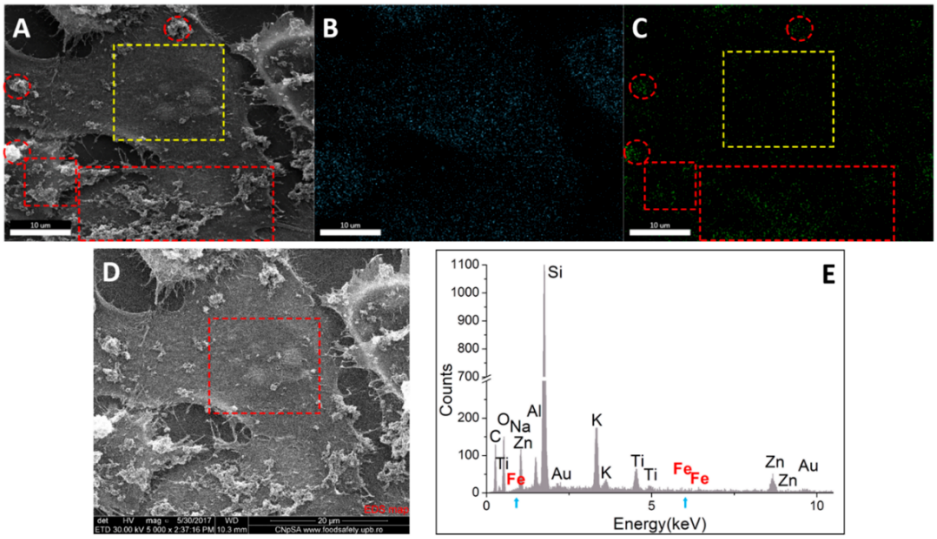

Fig. II.17. Qualitative and quantitative elemental characterization of MG-63 cells exposed to the highest concentration of Fe_3O_4@GEM during 24 h: (A) morphological image resulted using the signal resulted from secondary electrons (magnification 5000x); the red circles mark extracellular nanoparticle aggregates; the yellow square marks an area free of extracellular nanoparticle aggregates; (B) elemental mapping of C atoms in image A; (C) elemental mapping of Fe atoms in image A; (D) morphological image resulted using the signal resulted from scattered electrons (magnification 5000x); the red square marks the area which was subjected to the quantitative elemental analysis; (E) EDX spectrum for image D (red square); the blue arrows mark the absence of Fe in the area for which EDX analysis was done. [20]

In case of MG-63 cells (Fig. II.17), it is evidenced the disparity between the areas with Fe_3O_4@GEM extracellular aggregates (bounded by a yellow square). EDX mapping and EDX quantitative spectrums proved the absence of Fe from the selected area (yellow square), he green dots wih low intensity in Fig. II.34. C being determined by background noise. These

results sugest the fact that the nanoparticles were not internalized in MG-63 cells, the results being accordingly to the cell viability measurements, which proved reduced cytotoxic effects (Fig. II.14).

II.3.1.2. *In situ* doxorubicin functionalized Fe_3O_4 nanoparticles

The effect of doxorubicin (un)conjugated nanoparticles using the *in situ* method (Fe_3O_4 și Fe_3O_4@DOX) on the MG-63 human osteosarcoma cells were evaluated through the metabolic efficiency of these cells, by using the MTT tetrazolium salts test (Fig. II.18). Non-conjugated Fe_3O_4 did not prove any cytotoxicity for MG-63 cells at none of the analysed concentrations, because the viability of the cells exposed to bare NP was approximately 100%, compared to untreated cells. The toxicity in MG-63 cells exposed to Fe_3O_4@DOX decreased with concentration and exposure time. Fe_3O_4@DOX induced a significant decrease in MG-63 cells viability compared to control group, but also to the group exposed to unfunctionalized Fe_3O_4 in equivalent concentrations (according to Student test). Regarding the response of the cells to free DOX, the treatment during 24h determined a decease of the metabolic activity under 60%, effect significantly reduced compared to Fe_3O_4@DOX. After 48h of incubation in DOX presence, MG-63 cells proved an accentuated inhibition of cells viability for all employed concentrations. The MTT test results proved that, starting with 0,4 μg/mL equivalent concentation, a saturation of the cytotoxic effect takes place, the viability being maintained constant for the last employed concentration, at all time intervals.

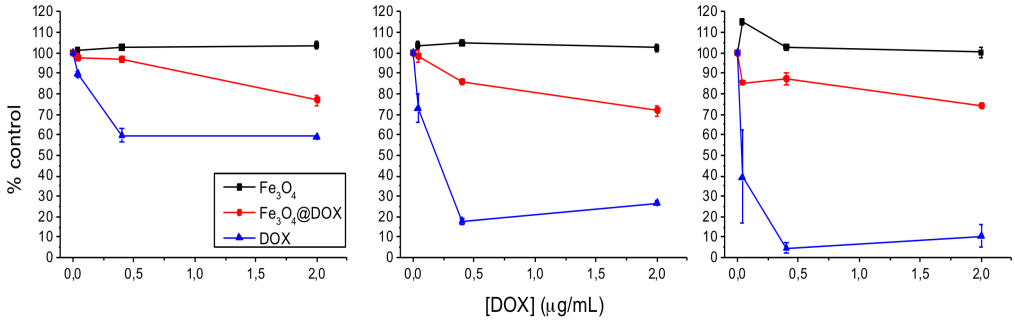

Fig. II. 18. MTT- MG-63 cells viability exposed to Fe_3O_4, Fe_3O_4@DOX and DOX in equivalent concentrations at time intervals of 24, 48, respectively 72 h; data is shown as mean±SEM; figure adapted after [24];

Cell death was quantified in order to give information regarding the mechanisms which arise. The measurements showed an increase in the number of apoptotic cells following the exposure to Fe_3O_4@DOX, depending on their concentration. The necrotic cell number in all groups exposed to nanoparticle treatment did not prove a statistically significant alteration, compared to control.

SEM was used to evaluate the detailed morphology of the MG-63 osteosarcoma cells exposed to Fe_3O_4@DOX, as well as their mechanism of interaction with the nanoparticles (Fig.II.19). The resulted images proved an alterated morphology and an increase in volume, by comparison to control cells. At this time interval, few nanoparticle aggregates were evidenced on the surface of the MG-63 cells (Fig. II.19. B), probably due to the internalization. This supposition was supported by the investigations performed in back scattered mode (Fig. II.19. F). Fe_3O_4@DOX nanoparticle aggregates directly interacted with cell membranes and the actin filaments ellongations in the extracellular medium, thus inducing a ruffling aspect at the membrane level (Fig. II.19. C, D). Vesicle-like structures were evidenced at the exterior of the MG-63 cells exposed to nanoparticles (Fig. II.19. B-D). SEM analysis proved that a possible

mechanism of the nanoparticles internalization could be macropinocytosis, due to the cell membranes aspect, but also due to the presence of macropinosomes [29].

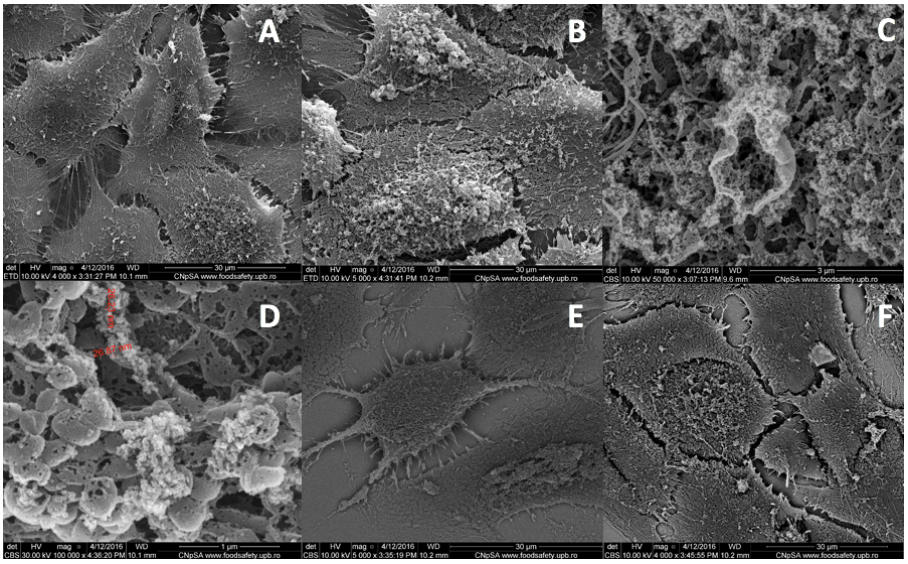

Fig. II.19. Scanning electron microscopy images for MG-63 osteosarcoma cells cultured during 48h: control (A,E) and in presence of Fe_3O_4@DOX in the highest concentration (B-D, F); the images were acquired using the information from secondary electrons (A-D), respectively scattered electrons (E-F); the images were acquired at different magnifications: 4000x (A, F), 5000x (B), 50000x (C) and 100000x (D); [24]

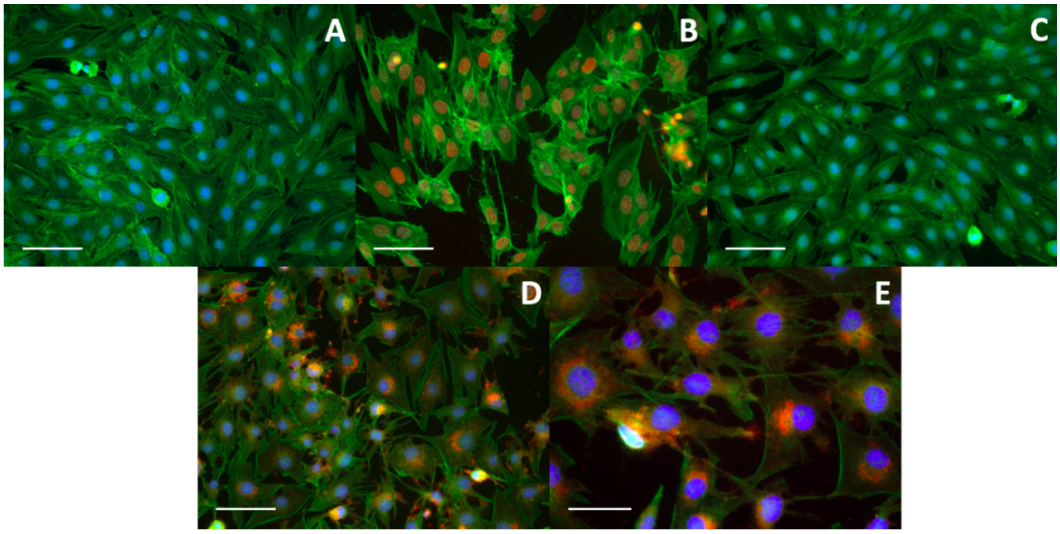

Fig. II.20. Fluorescence microscopy images for MG-63 osteosatcoma cells at 48h of culture in presence/ absence of nanoparticles: (A) control; (B) cells exposed to 2 μg/mL free DOX; (C) cells exposed to Fe_3O_4 in equivalent concentration of 2 μg/mL DOX; (D, E) cells exposed to Fe_3O_4@DOX in equivalent concentration of 2 μg/mL DOX; green: Phalloidin-FITC, blue: Hoechst, red: DOX; Scale in (A- D) is equivalent with 100 μm, respectively 50 μm in (E); figure adapted after [24];

Fluorescence images were done to evaluate the internalization process and localization of DOX, Fe_3O_4 and Fe_3O_4@DOX in osteosarcoma cells, but also to detect eventual morphological alterations (Fig. II.20). Fe_3O_4 nanoparticles up to 500 μg/mL concentration, did not induce any morphological alteration of MG-63 cells after 48h of exposure (Fig. 20.C). On the other hand, cells treated with DOX and Fe_3O_4@DOX showed morphological and structural alterations. The volume of osteosarcoma cells increased, while the cellular density decreased. Moreover, the actin fillaments lost their fibrillary structure (Fig. II.20. B, D, E). DOX is localized in the cell nucleus (Fig. II.20. B), while DOX conjugated nanoparticles are situated in the cytoplasm of the cells, in the peri-nuclear region (Fig. II.20. D, E).

Our data confirms a stable interaction between the organic and inorganic phases. The presence of the organic phase was proved through the termogravimetric analysis, but also through the prolongued fluorescence of the nano-construct, due to DOX native fluorescence. The direct conjugation of DOX with Fe_3O_4 nanoparticles facilitated the visualization of the nano-system location inside the cells. NPs are distributed in the cells cytoplasm, most probably in endosomes, while DOX enters in the nucleus through passive diffusion. The internalization mechanism of the nano-conjugate is different and takes place more slowly. Thus, at 48h of incubation, the nanoparticles are localized in the vicinity of the nucleus. Our results showed that DOX is delivered with a reduced speed from the nano-carrier, in physiologic conditions of pH, temperature and humidity, up to 72h.

II.3.2. Biological mechanisms evaluation of Fe_3O_4 nanoparticles used for the encapsulation of active substances

The evaluation of Fe_3O_4@PEG 6K (/DOX) internalization and cytotoxicity was assessed for human cervical adenocarcinoma HeLa cells. The nanoparticles visualization in HeLa cells after 16h of incubation in presence of NP was done using a Prussian blue staining, resulting a light blue coloring of the sub-micron structures localized mainly in the peri-nuclear area of the cells (Fig. II.21). Internalized Fe_3O_4@PEG 6K (/DOX) did not pass into the nucleus, remaining organized like aggregates covering the external nuclear membrane. The cells morphology was not affected in case of HeLa cells treated with DOX-free NP (Fig. II.21. C), however the cell density was altered due to the release of DOX from Fe_3O_4@PEG 6K/DOX in corresponding samples (Fig. II.21. B, D): cells seemed rounder and bigger in dimension, the nucleus volume increasing in size. The majority of the nanoparticle aggregates were localized inside the cells, perinuclearly, however some directly interacted with the exterior part of the membrane, following the internalization process. Complementarly, in case of Fe_3O_4@PEG 6K/DOX, the localization of the nano-constructs was confirmed through fluorescence microscopy, due to DOX native fluorescence property. These nanoparticles were organized like spherical sub-micron structures, localized especially in the peri-nuclear area, but also in the cytoplasm (Fig. II.21 E).

Transmission electron microscopy images were done for HeLa cells previously exposed to different concentrations of Fe_3O_4@PEG 6K (/DOX) (100 and 500 μg/mL) during 16h, in order to asses The NP internalization and intracellular localization. In Fig. II.22 is evidenced the internalization of Fe_3O_4@PEG 6K as aggregates in the peri-nuclear area and the cytoplasm. This observation was valid for all experimental conditions. Results proved that both type of constrcts are internalized through endocytosis and macropinocytosis (Fig. II. 22. D, C). After 16h of incubation with Fe_3O_4@PEG 6K, the NP seemed internalized in vesicles, eventually being transferred in lysosomes. Few Fe_3O_4@PEG 6K/DOX aggregates were localized in vesicle-like structures, most of them being free in the cytoplasm.

PIXE quantitative analysis (Fig. II.23) was done for Fe_3O_4 nanoparticles interacting with HeLa cells and proved an intracellular concentration of 31,66±3,06 pg Fe_3O_4/ cell for samples incubated with Fe_3O_4@PEG 6K and respectively 115,2±9,8 pg Fe_3O_4/ cell for Fe_3O_4@PEG 6K/DOX.

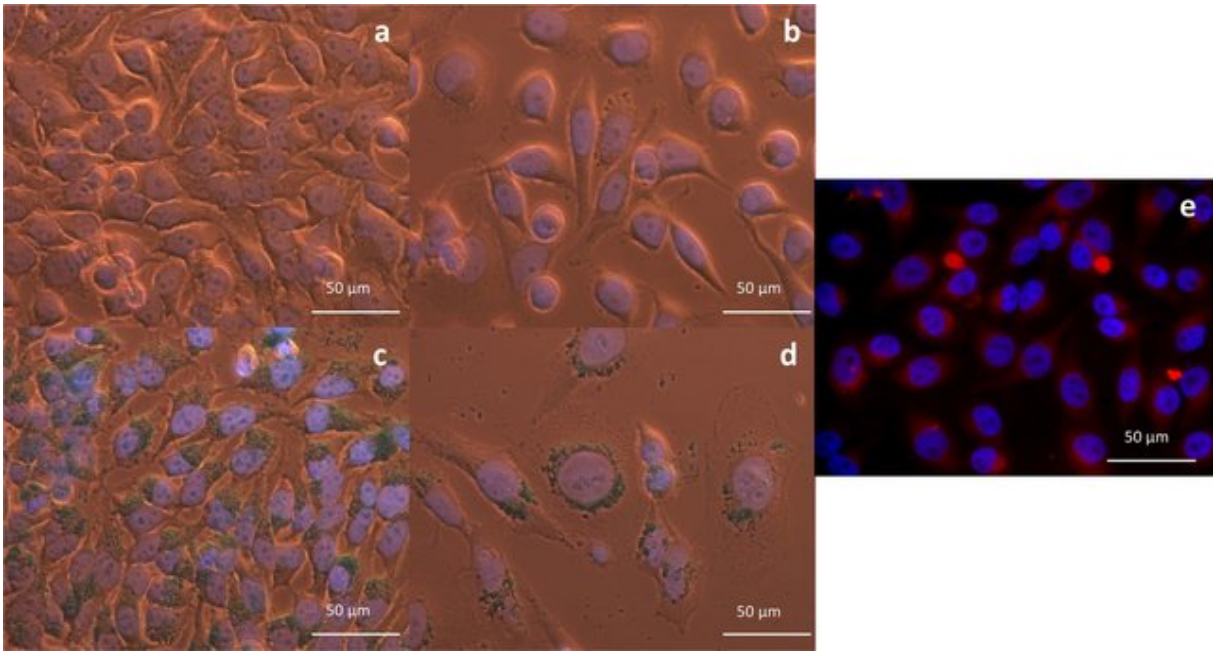

Fig. II.21. (A-D) Optical microscopy images of HeLa cells exposed during 16h to: (A) control cells; (B) DOX (1,11 µg/mL, equivalent concentration of Fe_3O_4@PEG 6K/DOX); (C) Fe_3O_4@PEG 6K (100 µg/mL) and (D) Fe_3O_4@PEG 6K/DOX (100 µg/mL); with blue are represented the iron oxide nanoparticles, due to Prussian blue staining; magnification 40x (oil). (E) Fluorescence microscopy images of HeLa cells exposed during 16h to 100 µg/mL Fe_3O_4@PEG 6K/DOX; with blue are represented the nuclei (marked with DAPI) and with red Fe_3O_4@PEG 6K/DOX or free DOX (due to DOX fluorescence); magnification 40x; [26].

Short term cytotoxicity measurements were done for a large concentration range of Fe_3O_4@PEG 6K (/DOX) nanoparticles (0-200 µg/mL, binary dillutions). For this, the mitochondrial metabolic potential was monitored through the cell viability test based on tetrazolium salts MTT (Fig. II.24) up to 96h of NP treatment. HeLa cells response to Fe_3O_4@PEG 6K depended more on time and less on the NP concentration (Fig. II.24). At 48h of exposure, Fe_3O_4@PEG 6K showed a slow decrease in cells viability, inversely proportional to NP concentration. At 96h of treatment, no significant alteration of the cells viability was observed, compared to control samples, with a maximum reduction of cell viability of 10,88±7,675 % for 200 µg/mL Fe_3O_4@PEG 6K. All results were statistically significant, compared to controls (untreated cells).

Results for Fe_3O_4@PEG 6K/DOX (Fig. II.24) proved that the NP cytotoxic effect for HeLa cells is directly proportional to NP concentration and exposure time. The calculated IC_{50} were 27,83±7,99 µg/mL at 48h, 2,31±0,32 µg/mL at 72h and 9,006± 4,68 µg/mL at 96h. All results were statistically significant, compared to controls (untreated cells), according to one-way ANOVA. Moreover, two-ways ANOVA statistical analysis proved a significant difference between the effects produced by Fe_3O_4@PEG 6K and Fe_3O_4@PEG 6K/DOX ($P<0,0001$ at 48h; $P<0,0001$ at 72h; $P<0,0001$ at 96h). Also, DOX presence in the nano-consruct induced a significant reduction of the cells viability ($P=0,0003$ at 48h; $P<0,0001$ at 72h; $P<0,0001$ at 96h).

In this study, iron oxide nanoparticles functionalized with polyethylene glycol were designed and synthesized (Fe_3O_4@PEG 6K) for the encapsulation of the chemotherapeutic substance DOX (Fe_3O_4@PEG 6K/DOX). The internalization mechanism of Fe_3O_4@PEG 6K (/DOX) in HeLa cells was done through pino and enocytosis, both NP accumulating in the peri-nuclear area. DOX free NP proved to be biocompatible for HeLa cells, while the cells treatment with Fe_3O_4@PEG 6K/DOX induced a decrease of proliferation dependent on the NP concentration an incubation time.

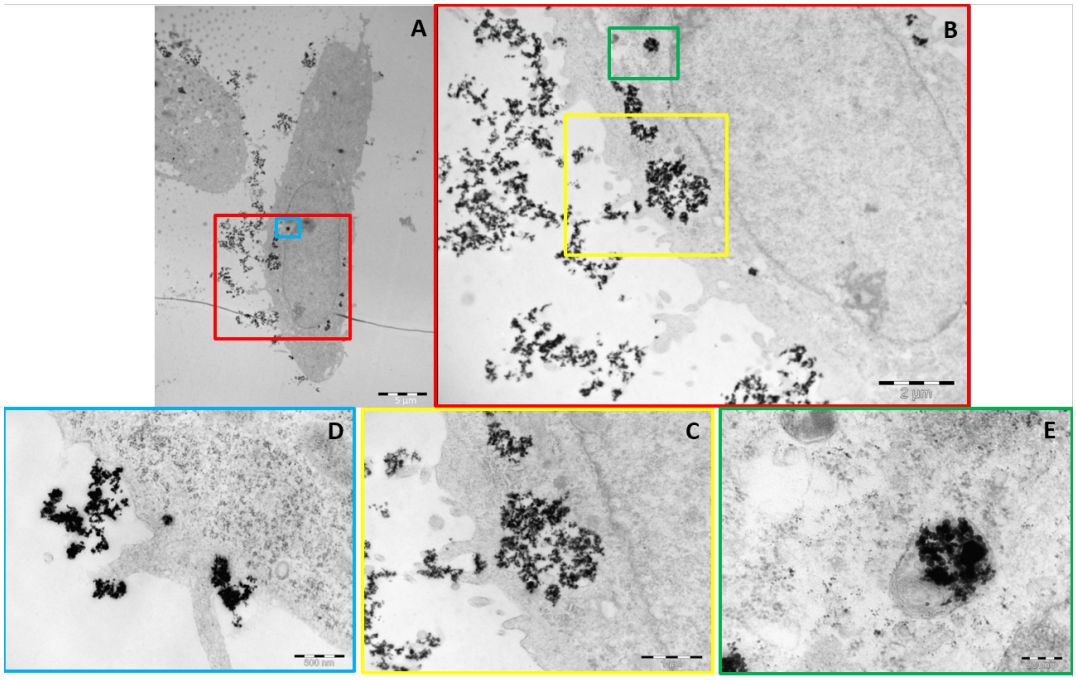

Fig. II.22. HeLa cells exposed to 100 μg/mL Fe_3O_4@PEG 6K during 16h: (A) whole cell visualisation; (B) magnification of the area marked with red square in (A); (C) magnification of the area marked with yellow square in (B); (D) magnification of the area marked with blue square in (A); and (E) magnification of the area marked with green square in (B); [26].

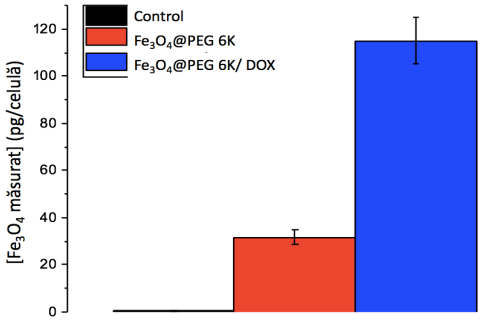

Fig. II. 23. Quantity of internalized Fe_3O_4 in HeLa cells incubated with 0, respectively with 100 μg/mL Fe_3O_4@PEG 6K (/DOX) during 16h, at 24h from NP removal; data is shown as mean±SEM (n=3); adapted from [26].

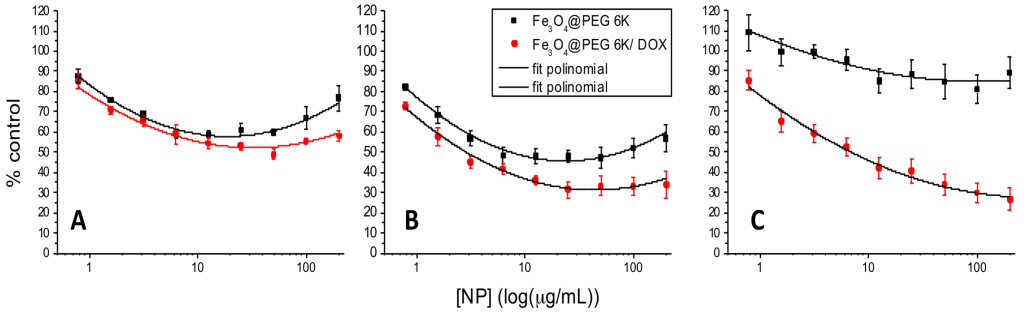

Fig. II.24. HeLa cells viability after incubation with Fe_3O_4@PEG 6K (/DOX) (in equivalent cocnentrations), determined at 48, 72, respectively 96h after tratament. Results are expressed as percent from control (untreated cells). Data is shown as mean ±SEM; adaptated from [26].

II.4. Contributions regarding the evaluation of Fe_3O_4 nanoparticles radiosensitization potential

II.4.1. Biological mechanisms evaluation involved in radiotherapy followed by Fe_3O_4 nanoparticles treatment

The potential cytotoxic effects of radiation treatment followed by exposure to Fe_3O_4@DOX in MG-63 humn osteosarcoma cells were evaluated through metabolic investigations (MTT assay), proliferative (MTT assay and Tripan blue staining), respectively genotoxic (micronucleus formation assay). MG-63 cells at confluency were irradiated with 1 Gy (150 KeV), allowed to attach during 4h and then exposed to different concentrations of Fe_3O_4@DOX in the range of 0-500 μg/mL.

Cells proved a significant reduction of MTT metabolic activity, accentuated for groups receiving both treatments (Fig. II.25). Thus, cells following exposure to 1Gy X-Rays and Fe_3O_4@DOX proved a statistically significant decrease in the cells ability to reduce the tetrazolium salt ability, which was dependent on the NP concentration. Complementarly, the clonogenic assay was done to evaluate the long term cytotoxicity of radiation followed by Fe_3O_4@DOX treatment (Fig. II.26). Cell survival decreased following radiation treatment, the effect being accentuated by the addition of 500 μg/mL NP for 48h (a total reduction of cells survival with 50,62±5,8%, compared to controlul). NP alone had an inhibitory effect on the MG-63 cells survival, depending on their concentration. A significant effect was evidenced for dual treatment using radiation (1 Gy X-Rays) and Fe_3O_4@DOX (500 μg/mL) on the cell survival fraction $P< 0,01$ (Fig. II.26).

The measurement of micronuclei production was done at 48h and 72h of NP treatment (Fig. II.27). Fe_3O_4@DOX did not induce any statistically significant alteration of the micronuclei index in MG-63 cells, for none of the concentration at 48 and 72h of treatment. As expected, the irradiation treatment induced chromosome fragmentation, measured as a significant increase of micronuclei index at 48h ($P<0,01$), respectively at 72h ($P<0,05$). For the groups exposed to ionizing radiation followed by NP administration, an increase in the micronuclei number was noticed, compared to control (untreated cells). However, Fe_3O_4@DOX did not induce any additional effect to radiation, rather the exposure to 1Gy X-Rays before NP treatment induced a statistically significant effect compared to samples exposed only to NP ($P<0,01$ for 100 μg/mL, respectively $P<0,001$ 500 μg/mL at 48h; $P<0,001$ for 100 μg/mL and $P<0,05$ for 500 μg/mL at 72h).

The potential mechanisms induced by ionizing radiation on the Fe_3O_4@DOX internalization in MG-63 cells were investigated. For this, quantitative measurements of atomic iron concentration in cells were correlated with cell cycle measurements.

PIXE technique was used to measure the atomic Fe concentration in MG-63 cell cultured in presence of Fe_3O_4@DOX nanoparticles during 24, respectively 48h, and previously exposed to different radiation doses (0 and 1 Gy) (Fig. II.28). Results proved that the exposure to NP induced an increase in atomic Fe concentration proportional with the administered NP quantity. At 48h, a concentration of 473,5±97,63 pg Fe_3O_4 /cell ($P<0,05$, compared to control) was measured in non-irradiated MG-63 cells treated with 500 μg/mL Fe_3O_4@DOX, respectively 860,15±52,36 pg Fe_3O_4 /cell ($P<0,001$, compared to control) for the equivalent group which received previous irradiation treatment. Thus, the exposure to 1Gy X-Rays determined a statistically significant increase of internalized NP quantity in MG-63 for the highest administered concentration (500 μg/mL), with $P<0,01$ compared to the equivalent non-irradiated group at 48h.

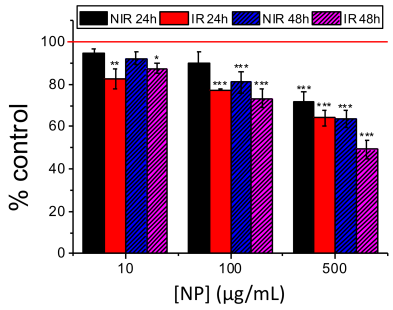

Fig. II.25. Viability of MG-63 cells exposed to different concentrations (0, 10, 100, 500 µg/mL) of Fe_3O_4@DOX during 24 and 48 h; a group of cells was exposed to 1 Gy X-Ray (IR) vs non-irradiated control (NIR); data is shown as mean ±SEM; *P<0,05 **P<0,01 and ***P<0,001; adapted from [24];

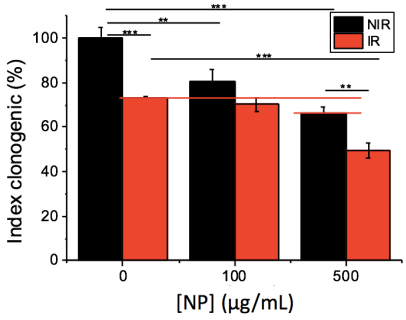

Fig. II.26. Cell survival of MG-63 previously exposed to 0Gy, 1Gy X-Rays, 500 µg/mL, 100 µg/mL Fe_3O_4@DOX or combined treatment, during 48h; data is shown as mean ±SEM; *P<0,05 **P<0,01 and ***P<0,001; adapted from [24];

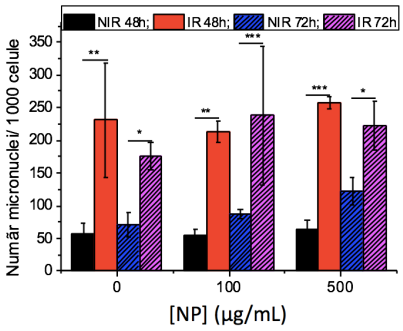

Fig. II.27. Micronuclei index in MG-63 cells exposed during 48, respectively 72h to Fe_3O_4@DOX; a group of cells was previously irradiated with 1 Gy X-Rays (IR); data is shown as mean ±SEM; *P<0,05 **P<0,01 and ***P<0,001; adapted from [24];

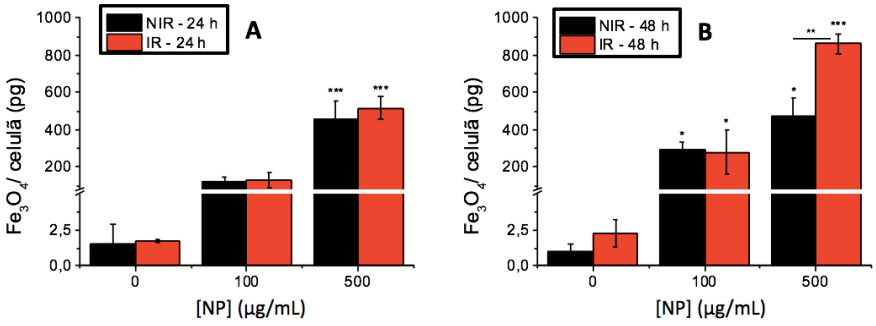

Fig. II.28. Quantity (pg) of internalized Fe_3O_4 in MG-63 osteosarcoma cells exposed to different concentrations of Fe_3O_4@DOX during 24, respectively 48h; a group of cells as previously exposed to 1Gy; data is shown as mean ±SEM; *P<0,05 **P<0,01 and ***P<0,001; adapted from [24];

MG-63 cells were culured at conflunency in order to increase the percent of cells in G_0/G_1 phase of the cell cycle and then exposed to 1Gy X-Rays. Cell detachment following irradiation and cell seeding did not induce any significant alterations of the cell cycle distribution at 4h (Fig. II.29). At this time interval, cells in corresponding groups were exposed to NP-containing cell culture medium at different concentrations. At 12h after X-Ray exposure, evident alterations of the cell cycle were noticed (Fig. II.29). X-Ray treatment induced an accumulation of the cells in G_2/M transition phase at 12h after irradiation (21,8±2,3%, P<0,05 compared to control), while NP alone did not induce any statistically significant effect. However, combined treatment determined the accumulation of a high percent of cells in the transition phase G_2/M (27,6±1,92, P<0,01 compared to control and P<0,05 compared to non-

irradiated NP treated cells). At 24h, approximately 30% of the cells were blocked in G_2/M phase in all investigated groups (with no statistically significant differences), proving that the cells probably escaped cell cycle blockage and underwent mitosis.

The type of cell death following ironizing radiation and Fe_3O_4@DOX exposure was investigated by using the clonogenic cell death assay (eg. Apopsisys, mitotic catastrophe, respectively senescence). Morphological evaluation of cell death (Fig. II.30) proved that, after 48h of NP treatment and after the subculturing of resistant clones for another 24h, the apoptosis wass not induced in any of the investigated groups, with the exception of 1Gy and 500 μg/mL Fe_3O_4@DOX. For cells exposed to 1Gy and 500 μg/mL Fe_3O_4@DOX, an increase of 2,34 times in the apoptotic cell number was noticed ($P<0,01$ compared to non-irradiated control). Seemingly, the combined treatment contributed to a statistically significant increase of mitotic catastrophe events in cells exposed to the highest concentration of nanoparticles ($P<0,05$). A lower percent of senescent cells was observed for cell populations exposed either to the highest concentration of nanoparticles, either to the combined treatment. Our results proved that the mitotic catastrophe cell death mechanism is the most frequently encountered in case of dual radiation-NP treatment. At 48h, these cells exis the G_2/M cell cycle phase (a lower percent of cells in G_2/M, similarly to control group) having unrepaired DNA and aberrant mitosis (multi-nucleate cells).

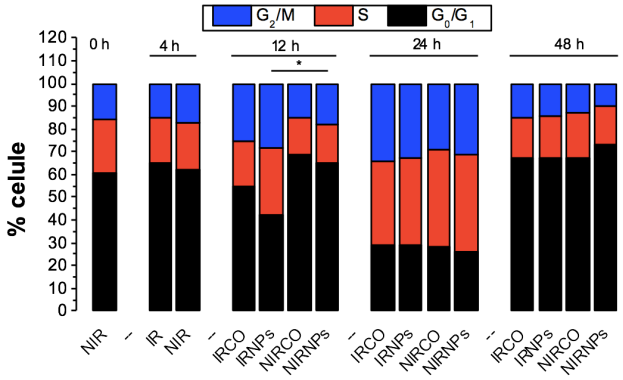

Fig. II.29. Cell cycle distribution for MG-63 cells exposed to radiation treatment (0, 1 Gy) and NPs (0, 500 μg/mL Fe_3O_4@DOX) at different time intervals; *P<0,05; adapted from [24];

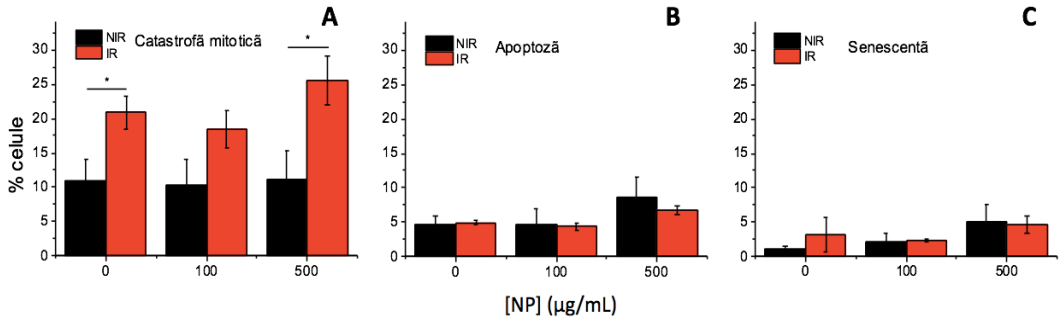

Fig. II.30. Clonogenic cell death induced by 1 Gy X-Rays, 500 μg/mL, respectively 100 μg/mL Fe_3O_4@DOX, or combined treatment; cells were treated during 48h and re-seeded for 24h; data is shown as mean ±SEM; *P<0,05; adapted from [24];

In this study we have used medium dose X-Rays to sensizite osteosarcoma cells at confluency for Fe_3O_4 nanoparticles *in situ* conjugated with doxorubicin. We have proved that the combined treatment induced an increase of the cytotoxic and genotoxic effects in osteosarcoma cells, compared to NP alone. Our results showed that the temporary cell cycle arrest in G_2/M for cells previously exposed to 1Gy X-Rays was associated to an enhanced internalization of Fe_3O_4@DOX. The group receiving both 1Gy and 500 μg/mL NP treatment

occurred an early G_2/M induction at 12h from irradiation, reaching a maximum at 24h after treatment, when all cell groups entered this cell cycle phase.

II.4.2. Biological mechanisms evaluation involved in Fe_3O_4 nanoparticles mediated radiotherapy

In order to evaluate the radiosensitization potential of Fe_3O_4@PEG 6K(/DOX) nanoparticles, bidimensional cell cultures of two tumor cell lines (scuamos cell carcinoma FaDu, respectively human cervical adenocarcinoma HeLa) and a normal cell line (human ketatinocytes HaCat) were incubated with NP during 16h and then irradiated. X-Rays with different energies were used: high energy (6MV), as well as medium (150 kV) and low energies (50 kV), because they have a different clinical relevance.

The long term response to nanoparticles followed by ionizing radiation was evaluated using the clonogenic test, to reveal possible effects of chemo- and radio-sensitization. By incubating HeLa cells with100 µg/mL Fe_3O_4@PEG 6K/DOX during 16h a significant decrease in HeLa cells survival was determined compared to control (SF(Fe_3O_4@PEG 6K /DOX) = 0,56 ± 0,14, P=0,04), but this effect was not obtained for Fe_3O_4@PEG 6K, showing the biocompatibility of drug free nanoparticles (Fig. II.31).

The exposure of HeLa cells to a concentration of 100 µg/mL Fe_3O_4@PEG 6K before irradiation at a 6MV energy did not induce any statistically significant effect compared to radiation alone for none of the applied doses, except for 8Gy, where the clonogenic survival in the group receiving both treatments was lower than control (P=0,04, fig. II.31). On the other hand, the radio-sensizing effect of DOX free NP (100 µg/mL) was evidenced for low energy X-Rays (50 kV), a low surviving rate of Hela cells being significantly reduced compared to control cells in equivalent groups, at 4 and 5 Gy (Fe_3O_4@PEG 6K vs control: P=0,03, P=0,04, Fig. II.32). Incubation with Fe_3O_4@PEG 6K during 16h before irradiation with 50 kV induced a radiosensiziting effect with a calculated dose modifying factor for a survivinf rate of 0,1 $DMF_{SF\ 0.1}$= 1,13 ±0,05.

The incorporation of DOX in NP determined the clonogenic inactivation of cervical adenocarcinoma cells exposed to dual treatment (NP and radiation). The dose modifying factor in case of HeLa cells incubated during 16h with 100 µg/mL Fe_3O_4@PEG 6K/DOX and then irradiated with different doses (0-8 Gy), at an energy of 6 MV, was $DMF_{SF\ 0.1}$= 1,3 ±0,1. These observations suggested that the decreasing effect of HeLa cells survival rate was determined by an additive cytotoxic effect of DOX, rather than a radiosensitizing effect of 6MV radiation therapy.

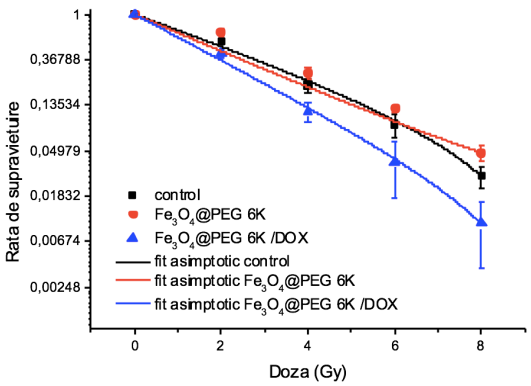

Fig. II.31. Clonogenic survival rate of HeLa cells exposed to 100 µg/mL Fe_3O_4@PEG 6K(/DOX) during 16h and followed by 6MV X-

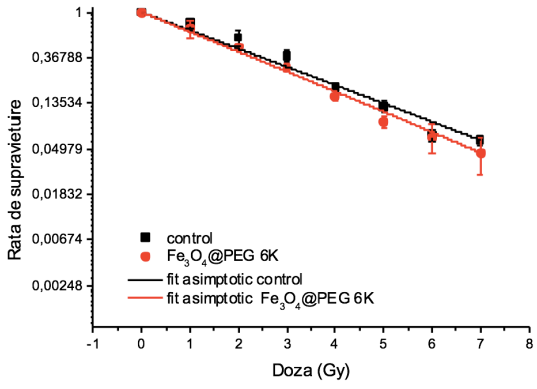

Fig. II.32. Clonogenic survival rate of HeLa cells exposed to 100 µg/mL Fe_3O_4@PEG 6K during 16h and followed by 50kV X-Ray

Ray exposure. Data is shown as mean ±STDEV (n=3);

exposure. Data is shown as mean ±STDEV (n=3);

Irradiation with 150 kV of HeLa cells following the incubation with 100 μg/mL Fe_3O_4@PEG 6K/DOX determined a significant decrease of clonogenic indext at 4 Gy (P<0,01, Fig. II.33) with a $DMF_{SF=0,1}$=1,29±0,04. Similarly, the incubation with 200 μg/mL NP induced a significant clonogenic inactivation at 4Gy (P=0,01, Fig. II.33) with a $DMF_{SF=0,1}$=1,55±0,12.

Incubation of FaDU squamous cell carcinoma cells with Fe_3O_4@PEG 6K /DOX did not determine any significant alteration of the cell survival rate after exposure to different doses of 150 kV X-Rays, at none of the investigated concentrations, suggesting that the radio-modulatory effect of these nanoparticles depends on the cell type. Regarding the cell response to 150 kV ionizing radiation, the 2D normal cell model of human keratinocytes (HaCat) proved an increased radio-resistance, compared to the investigated tumor models. Incubation with Fe_3O_4@PEG 6K /DOX during 16h before irradiation had a radio-protective effect.

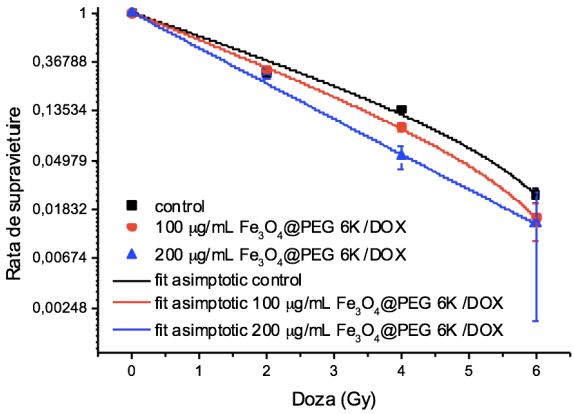

Fig. II.33. Clonogenic survival of HeLa cells exposed to 0, 100, respectively 200 μg/ mL Fe_3O_4@PEG 6K/DOX during 16h and followed by 150 kV X-Ray at different doses; data is shown as mean ± STDEV (n=3);

Nanoparticles internalization in all 3D tumor models was done as a concentration gradient starting from exterior the upper part of the spheroid, towards its center and the opposite side, by following the gravitational force. The maximum degree of nanoparticle penetration towards the middle of the speroids was observed at 48h of incubation for both tumor models. This time interval was selected for subsequent irradiation experiments. In case of 3D cell models of human cervical adenocarcinoma, the nanoparticles were especially localized in the area of proliferating cells (in S phase of the cell cycle). On the other hand, in case of FaDu model, Fe_3O_4@PEG 6K /DOX were internalized in cells in the proliferating area, as well in cells in the hypoxic area.

The response of the cells in 3D cell models to NP and radiation treatment was different from the response of the cells in 2D cell models. Thus, in case of HeLa 3D model, was obtained a $DMF_{SF=0,1}$ = 1,08 for 100 μg/mL, respectively $DMF_{SF=0,1}$ = 1,09 for 200 μg/mL (Fig. II.34), while for FaDu 3D cell model, the nanoparticles rather proved a radio-protective effect (Fig. II.35). Two-ways ANOVA test proved that the results are statistically significant, by means of dose variation, but not by the NP concentration. Fisher test confirmed these observations and, additionally showed that the incubation of the HeLa spheroids with nanoparticles induced a statistically significant radio-sensitizing effect for 200 μg/mL NP.

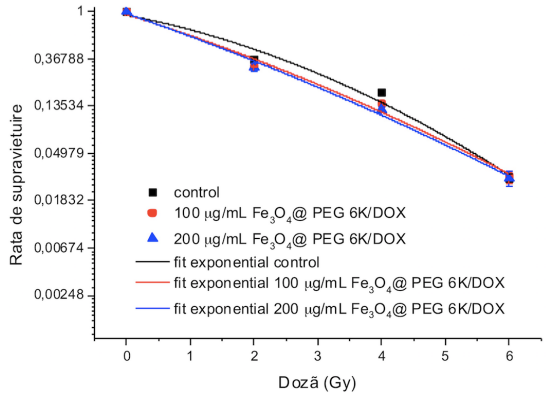

Fig. II.34. Clonogenic survival of HeLa cells cultured in a 3D model and exposed to 0, 100, respectively 200 μg/ mL Fe_3O_4@PEG 6K/DOX during 16h followed by 150 kV X-Ray at different doses; data is shown as mean ± SEM (n=3);

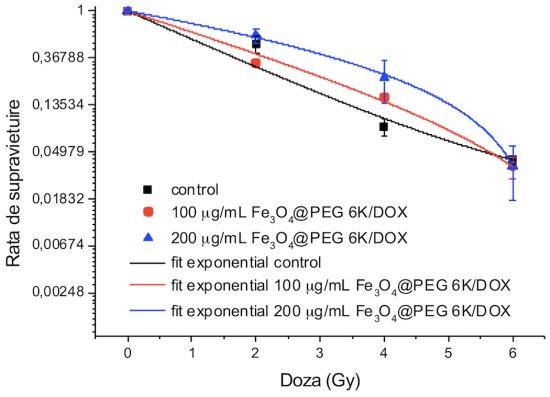

Fig. II.35. Clonogenic survival of FaDu cells cultured in a 3D model and exposed to 0, 100, respectively 200 μg/ mL Fe_3O_4@PEG 6K/DOX during 16h followed by 150 kV X-Ray at different doses; data is shown as mean ± SEM (n=3);

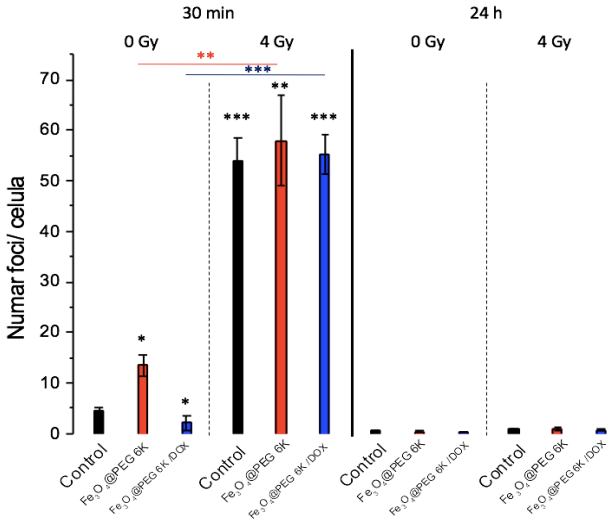

Fig. II.36. DNA lesions measured through γ-H2Ax foci, induced by treatment with 100 μg/mL Fe_3O_4@PEG 6K (/DOX) during 16h and/or 4Gy 6MV; measurements were done at 30 min and respectively at 24 h after radiation treatment;

Possible mechanisms of ionizing radiation cytotoxicity, the frequency of DNA double strand breaks in human cervical adenocarcinoma cells exposed to Fe_3O_4@PEG 6K(/DOX) and 4 Gy 6 MV X-Rays was quantified (Fig. II.36). Following the incubation during 16h with NP and no radiation treatment, a high number of γ-H2AX foci per cell was obtained in case of Fe_3O_4@PEG 6K, as well as Fe_3O_4@PEG 6K/DOX, ($P<0,05$, compared to control cells Fig. II.36). The exposure to 4 Gy 6 MV X-Rays determined an increase in γ-H2AX foci/ cell, immediately after irradiation (30 min). At 24h from radiation treatment the measurements proved no significant alterations of the double strand breaks index for none of the investigated conditions (Fig. II.36). FACS measurements of the cell cycle proved that the irradiation of cells induced a statistically significant alteration of the cell cycle distribution, confirmed using two-ways ANOVA test. The incubation with nanoparticles before 6MV ionizing radiation treatment did not influence this effect. Thus, the radiosensizitation mechanisms in cells exposed to Fe_3O_4@PEG 6K(/DOX) were not correlated with the induction of DNA double strand breaks, nor with alterations of the cell cycle.

III. General conclusions

The first chapter ("Critical literature study") does a review summary of the current progress regarding the applicability of Fe_3O_4 nanoparticles in nanomedicine. Magnetite nanoparticles (Fe_3O_4) are well known for their magnetic properties, but in addition to these are friendly with tissues biological fluids, their biocompatibility determining their applications in numerous medical domanis such as controlled delivery of active substances, cancer treatment through magnetic hyperthermia, use as contrast substance in medical imaging, biofilm inhibition and radiosensitization.

The second chapter ("Personal contributions") contains the results regarding the obtaining, conjugation and evaluation of magnetite nanoparticles as chemo- and radio-sensitizers for *in vitro* preclinical models. The co-precipitation method was used to synthesize the Fe_3O_4 nanoparticles, because of its advanages such as ease, reproducibility, high yield synthesis. Following synthesis, the resulted homogenous nanoparticles (by means of morphology and composition) were characterized by a high crystallinity degree.

This method can be altered in order to apply an *in situ* functionalization. Thus, magnetite nanoparticles *in situ* functionalized with anti-tumor drug (gemcitabine or doxorubicine) had a high degree of hydrodynamic stability. Moreover, Fe_3O_4@GEM proved a cemical potentiating effect of GEM cytotoxic effects for tumor cells BT474 breast ductal carcinoma and respectively HepG2 hepatocellular carcinoma, but not for MG-63 human osteosarcoma. A similar effect was observed for Fe_3O_4@DOX and DOX. The nanoparticles were internalized through macropinocytosis in MG-63 cells, while DOX was internalized through direct diffusion in the nucleus. On the other hand, post-synthesis conjugation of magnetite nanoparticles with DOX lead to the inneficient loading of the drug, proved through spectrophotometric investigations, but also through biological investigations using fluorescence microscopy.

By the functionalization of magnetite nanoparticles with PEG, an increase in DOX quantity interacting with the NP increased. The molecular weight of PEG influenced the morphology and homogeneity of the resulting nanoparticles following the *in situ* conjugation of Fe_3O_4, but also the encapsulated DOX quantity. By means of morphological homogeneity and biological investigations, the 6000 Da PEG *in situ* conjugated samples showed the best results.

The post-synthesis functionalization of Fe_3O_4 nanoparticles determined the encapsulation of a high quantity of anti-tumor drug compared to samples obtained through *in situ* conjugation. *In vitro* biological testing performed on human cervical adenocarcinoma HeLa cells proved that Fe_3O_4@PEG 6K were efficiently internalized through macropinocytosis and endocytosis. The nanoparticles were efficient in the encapsulation and direct delivery of DOX in the cytoplasmic compartment, leading to the cellular death of HeLa.

The implication of magnetite nano-systems in the dual treatment of cancer involving radiotherapy and chemotherapy was evaluated through the monitorization of cytotoxic effects by applying the ionizing radiation treatment before or following the incubation of cells with nanoparticles.

In the first case, was investigated the correlation between the increase of Fe_3O_4@DOX NP internalization following the irradiation of the cells with the cell cycle progression, as well as the characterization of the cyto- and genotoxicity degrees and the identification of cell death type. A higher significant percent of magnetite nanoparticles was measured in cells that were irradiated previous to NP exposure, phenomena associated with a more rapid entrance of the cells in the G_2/M phase of the cell cycle. The resumption of the normal cell cycle at 48h of treatment was correlated with morphological observations regarding the alterations of the nuclei of the osteosarcoma cells occurring mitotic catastrophe.

On the other hand, the incubation of the tumor cells with Fe_3O_4@PEG 6K (/DOX) nanoparticles followed by irradiation at different energies and doses proved a radio-sensitization effect dependent on the concentration of the nanoparticles, concentration of DOX,

but also the energy and dose of ionizing radiation. Moreover, the effect was different for different tumor and normal cell lines. The obtained results proved that DOX free Fe_3O_4@PEG 6K determined a decrease of cell curvival in 2D HeLa cells following the radiation with low energy X-Rays (50 kV), but not following radiation with high energy (6MV). Through DOX encapsulation, a radio-sensitizing effect was obtained on HeLa cells at both high (6MV) and medium (150 kV) energies, evidenced in 2D and 3D cell models. The phenomenon was not correlated with the production of double strand DNA, nor with significant alterations of the cell cycle. The radio-modulatory cytotoxic activity was not observed for the tumor cell line squamous cell carcinoma FaDu (2D and 3D) and neither for the normal cell line human keratinocytes HaCat, the results rather showing a protective effect against X-Rays.

Results proved the efficiency of functionalized magnetite nanoparticles in the controlled delivery of anti-tumor substaced and the chemical and/or radiological sensitization of human tumor cells. These observations confirm the potential use of the resulted nano-sysntems as potential candidates in the chemo- and radio-therapy mediated by nanoparticles.

Novelty elements of the thesis:

- We have obtained and reported for the first time Fe_3O_4 nanoparticles directly conjugated with the anti-tumor drug gemcitabine and respectively doxorubicin, by employing an *in situ* functionalization method.
- We have used the EDX elemental mapping technique correlated with SEM in order to evaluate the internalization of Fe_3O_4@GEM and their interaction with cell membranes.
- We have used STEM and single point EDX techniques to evaluate the cellular internalization of NP without a previous sectioning of the cells.
- We have characterized the mitotic catastrophe mechanism of radio-resistant MG-63 cells associated with an increased effect of Fe_3O_4@DOX nanoparticles internalization following irradiation.
- We have used a co-precipitation method adapted to room temperature associated with post-synthesis encapsulation in PEG, resulting core-shell highly crystalline magnetite nanoparticles.
- We have reported the first study regarding the intracellular retaining of the PEG functionalized Fe_3O_4 nanoparticles; the mechanisms were evaluated qualitatively through microscopy techniques and quantitatively through spectrometry techniques for different time intervals higher than a complete cell cycle after the exposure of the NP was interrupted.
- We have used for the first time DOX delivery systems based on magnetite nanoparticles encapsulated in PEG in order to radiosensitize the tumor cells. We have reported a significant radio-modulatory effect in 2D and 3D cell cultures. These effects were associated with the localization of the NP at cytoplasmic level.

IV. Results dissemination

Articles published in internationally indexed publications as first author:

[1] ***R.C. Popescu***, *M. Straticiuc, C. Mustaciosu, M. Temelie, R. Trusca, B.S. Vasile, A. Boldeiu, D. Mirea, R.F. Andrei, C. Cenusa, L. Mogoanta, G.D. Mogosanu, E. Andronescu, M. Radu, M.R. Veldwijk, D.I. Savu*, "Enhanced Internalization of Nanoparticles Following Ionizing Radiation Leads to Mitotic Catastrophe in MG-63 Human Osteosarcoma Cells." Int J. Molec. Sci., 2020, **vol. 21**, nr. 19, 7220.

[2] ***R.C. Popescu***, *D. I. Savu, A.D. Olarescu, O. Gherasim, S. Banita, M. Straticiuc, D. Mirea, R.F. Andrei, R. Trusca, B.S. Vasile, G. Socol, E. Andronescu*. "In vitro magnetic targeted

delivery of doxorubicin using iron oxide nanoparticles leads to enhanced cell death in glioblastoma"in U.P.B. Sci. Bull, Series B, **accepted for publication**, 2020.

[3] ***R.C. Popescu***, *D. Savu, I. Dorobantu, B.S. Vasile, H. Hosser, A. Boldeiu, M. Temelie, M. Straticiuc, D.A. Iancu, E. Andronescu, F. Wenz, F.A. Giordano, C. Herskind, M.R. Veldwijk*. "Efficient uptake and retention of iron oxide-based nanoparticles in HeLa cells leads to an effective intracellular delivery of doxorubicin."in Sci. Rep., **vol. 10**, 2020, 10530.

[4] ***R.C. Popescu***, *E. Andronescu, B.S. Vasile.* "Recent Advances in Magnetite Nanoparticle Functionalization for Nanomedicine"in Nanomaterials (Basel), **vol. 9,** nr. 12, 2019, 1791.

[5] ***R.C. Popescu***, *E. Andronescu, B.S. Vasile, R. Trusca, A. Boldeiu, L. Mogoanta, G.D. Mogosanu, M. Temelie, M. Radu, A.M. Grumezescu, D. Savu.* "Fabrication and Citotoxicity of Gemcitabine-Functionalized Magnetite Nanoparticles"in Molecules, **vol.22**, nr. 7, 2017, 1080.

Articles published in internationally indexed publications as corresponding author:

[1] *M. Temelie,* ***R.C. Popescu****, D. Cocioaba, B.S. Vasile, D. Savu*. "Biocompatibility study of magnetite nanoparticle synthesized using a green method"in Rom. J. Phys. **vol. 63**, 2018, 703.

Book chapters published at international publishing houses as first author:

[1] ***R.C. Popescu***, *E. Andronescu, A.M. Grumezescu*. "In vitro and in vivo technologies: an up to date overview in tissue engineering" in Materials for Biomedical Engineering, edited by Alina-Maria Holban and Alexandru Mihai Grumezescu, Elsevier, 2019, pp. 463-484, ISBN 9780128169094.

[2] ***R.C. Popescu***, *D. Popescu, A.M. Grumezescu*. "Applications of rubber-based blends" in Recent Developments in Polymer Macro, Micro and Nano Blends, edited by P.M. Visakh, Gordana Markovic and Daniel Pasquini, Woodhead Publishing, 2017, Pages 75-109, ISBN 9780081004081.

[3] ***R.C. Popescu***, *O. Fufa, A.I. Apostol, D. Popescu, A.M. Grumezescu, E. Andronescu*. "Chapter 9 - Antimicrobial Thin Coatings Prepared by Laser Processing" in Nanostructures for Antimicrobial Therapy, Micro and Nano Technologies, Elsevier, 2017, Pages 223-236, ISBN 9780323461528.

[4] **R.C. Popescu**, M.O.M. Fufă, A.M. Grumezescu, A.M. Holban. "12 - Nanostructurated membranes for the microbiological purification of drinking water" In Water Purification, Academic Press, 2017, Pages 421-446, ISBN 9780128043004.

Articles published in internationally indexed publications as co-author:

[1] *A. Bragaru, M. Simion, I. Mihalache, A. Radoi, M. Banu, P. Varasteanu, P. Nadejde, E. Vasile, M.A. Acasandrei,* ***R.C. Popescu****, D. Savu, K. Mihaela*. "Comparative analysis of honey and citrate stabilized gold nanoparticles: In vitro interaction with proteins and toxicity studies"in J. Photochem. Photobiol. B Biol., **vol. 197**, 2019, 111519.

[2] *A.I. Visan, G. Popescu-Pelin, O. Gherasim, V. Grumezescu, M. Socol, I. Zgura, C. Florica,* ***R.C. Popescu****, D. Savu, A.M. Holban, R. Cristescu, C.E. Matei, G. Socol*. "Laser processed antimicrobial nanocomposite based on polyaniline grafted lignin loaded with Gentamicin-functionalized magnetite"in Polymers, **vol. 11**, nr. 2, 2019, 283.

[3] *I. Negut, V. Grumezescu, A. Ficai, A.M. Grumezescu, A.M. Holban,* ***R.C. Popescu****, D. Savu, B.S. Vasile, G. Socol.* "MAPLE deposition of Nigella sativa functionalized Fe_3O_4 nanoparticles for antimicrobial coatings"in Appl. Surf. Sci., **vol. 455**, 2018, pp. 513-521.

[4] *G. Popescu-Pelin, O. Fufă, **R.C. Popescu**, D. Savu, M. Socol, I. Zgură, A.M. Holban, B.S. Vasile, V. Grumezescu, G. Socol*. "Lincomycin–embedded PANI–based coatings for biomedical applications" in Appl. Sur. Sci., **vol. 455**, 2018, pp. 653-666.

[5] *D. Ficai, V. Grumezescu, O. Fufă, **R. Popescu**, A. Holban, A. Ficai, A. Grumezescu, L. Mogoanta, G. Mogosanu, E. Andronescu*. "Antibiofilm coatings based on PLGA and nanostructured cefepime-functionalized magnetite"in Nanomaterials, **vol. 8**, nr. 9, 2018, 633.

[6] *I.A. Păun, **R.C. Popescu**, B. Ş. Călin, C.C. Mustăciosu, M. Dinescu, C.R. Luculescu*. "3D biomimetic magnetic structures for static field stimulation of the osteogenesis"in Int. J. Molec. Sci., **vol. 19**, nr. 2, 2018, 495.

[7] *I.A. Păun, **R.C. Popescu**, C.C. Mustăciosu, M. Zamfirescu, B.Ş. Călin, M. Mihăilescu, M. Dinescu, A. Popescu, D.G. Chioibaşu, M. Sopronyi, C.R. Luculescu*. „Laser-direct writing by two-photon polymerization of 3D honeycomb-like structures for bone regeneration"in Biofabrication, **vol. 10**, nr. 2, 2018, 025009.

[8] *P.C. Balaure, B. Boarca, **R.C. Popescu**, D. Savu, R. Trusca, B.Ş. Vasile, A.M. Grumezescu, A.M. Holban, A. Bolocan, E. Andronescu*. "Bioactive mesoporous silica nanostructures with anti-microbial and anti-biofilm properties"in Int. J. Pharmaceutics, **vol. 531**, nr. 1, 2017, pp. 35-46, ISSN 0378-5173.

Book chapters published at international publishing houses as co-author:

[1] *O. Gherasim, **R.C. Popescu**, T.G. Gherasim, V. Grumezescu, E. Andronescu*. "Pharmacotherapy and nanotechnology" in Nanoparticles in Pharmacotherapy, edited by Alexandru Mihai Grumezescu, William Andrew Publishing, 2019, pp. 1-21, ISBN 9780128165041.

[2] *O. Fufă, **R.C. Popescu**, T.G. Gherasim, A.M. Grumezescu, E. Andronescu*. "Chapter 16 - Silver-based nanostructures for cancer therapy" in Nanostructures for Cancer Therapy, Micro and Nano Technologies, edited by A. Ficai and A.M. Grumezescu, Elsevier, **2017**, Pages 405-428, ISBN 9780323461443.

[3] *M.O.M. Fufă, **R.C. Popescu**, A.M. Grumezescu, A.M. Holban*. "7 - Microorganisms: new trends in environment-friendly and energy-saving water purification" in Water Purification, Academic Press, 2017, pp. 263-288, ISBN 9780128043004.

Conferințe naționale și internaționale:

[1] ***R.C. Popescu**, A.D. Olarescu, O. Gherasim, S. Banita, M. Straticiuc, D.A. Mirea, R.F. Andrei, B.S. Vasile, G. Socol, E. Andronescu, D.I. Savu.* "In vitro magnetic targeted delivery of doxorubicin using iron oxide nanoparticles leads to enhanced cell death"8th International Conference on Radiation in Various Fields of Research, RAD2020, 20-24 Iulie 2020, Virtual Participation; prezentare de tip poster.

[2] ***R.C. Popescu**, V. Kopaz, H. Hosser, F. Schneider, E. Andronescu, F. Wenz, F. Giordano, C. Herskind, W. Doerr, M.R. Veldwijk, D. Savu*. "Drug delivery nanosystems for intracellular release of doxorubicin improved the clonogenic inactivation of X-Rays in human cervical adenocarcinoma cells", 8th International Conference on Radiation in Various Fields of Research, RAD2020, 20-24 Iulie 2020, Virtual Participation; prezentare orală.

[3] ***R.C. Popescu**, M. Straticiuc, D. Mirea, R.F. Andrei, C. Mustaciosu, R. Trusca, B.S. Vasile, E. Andronescu, M. Radu, M.R. Veldwijk*. "Enhanced Internalizing of Nanoparticles Following Ionizing Irradiation Leads to Mitotic Catastrophe in Human Osteosarcoma Cells"Conferința Națională de Biofizică CNB2020, 14-16 Iunie 2020, Brasov, Romania; prezentare de tip poster.

[4] ***RC Popescu**, D Savu, I Dorobantu, BS Vasile, H Hosser, F Schneider, A Boldeiu, E Andronescu, F Wenz, FA Giordano, C Herskind, MR Veldwijk*. "Radiation Sensitization of Tumor Cells by Intracellular Accumulation of Doxorubicin by using Iron Oxide

Nanoparticles"Strahlentherapie und Onkologie, Springer Heidelberg, vol. 195, S92-S93; prezentare de tip poster.

[5] ***RC Popescu***, *D Savu, I Dorobantu, BS Vasile, H Hosser, F Schneider, A Boldeiu, E Andronescu, F Wenz, FA Giordano, C Herskind, MR Veldwijk*. "Radiosensitization of Tumor Cells by Intracellular Delivery of Doxoubicin Using Novel Iron Oxide-based Nanoconstructs"Int J. Rad. Oncol. Biol. Phys., vol. 105, nr. 1, E681; prezentare de tip poster.

[6] ***R.C. Popescu***, *D. Savu, I. Dorobantu, B.S. Vasile, H. Hosser, F. Schneider, A. Boldeiu, E. Andronescu, F. Wenz, C. Herskind, M.R. Veldwijk*. "Intracellular delivery of doxorubicin by novel ion oxide- based nano- constructs improves cytotoxic effects of ionizing radiation in human cervical adenocarcinoma cells" 2018 Jahrestagung Gesellschaft für Biologische Strahlenforschung; prezentare de tip poster.

[7] ***R.C. Popescu***, *I. Dorobantu, B.S. Vasile, H. Hosser, F. Schneider, E. Andronescu, F. Wenz, C. Herskind, D.I. Savu, M.R. Veldwijk*. "Can we use nanoparticles to improve radiation therapy?"Radiobiology Satellite Meeting of the 15th National Conference of Biophysics, Magurele, România, Septembrie 2018; prezentare de tip poster.

[8] ***R.C. Popescu***, *E. Andronescu, M. Straticiuc, C. Mustaciosu, M. Temelie, L. Mogoanta, G.D. Mogosanu, B. Vasile, A. Boldeiu, A.M. Grumezescu, M. Radu, M.R. Veldwijk, D. Savu*. "Low dose radiotherapy enhances iron oxide nanoparticles internalizing and toxicity for MG-63 osteosarcoma cells", The 44th Annual Meeting of the European Radiation Research Society, Pecs, Ungaria, 21-25. 08.2018; prezentare de tip poster.

[9] ***R.C. Popescu***, *E. Andronescu, D. Savu, M. Straticiuc, A.I. Apostol, C.C. Mustaciosu, G. Voicu, G.D. Mogosanu, I. Mindrila, B. Vasile, A.M. Grumezescu*. "Enhancement of entrapment and toxicity of doxorubicin-functionalized iron oxide nanoparticles for MG-63 cells using low dose radiotherapy", JINR 8th International Student Summer School «Nuclear Physics - Science and Applications, Brasov, Romania, 26 July- 4 August, 2017; prezentare orală.

[10] ***R.C. Popescu***, *E. Andronescu, M. Straticiuc, B.S. Vasile, A.M. Grumezescu, M. Veldwijk, D. Savu*. "In vitro biological testing of novel multifunctional nanosystems for chemo-sensitizing of tumor cells" JRC Summer School on Alternative Approaches for Risk assessment, Joint Research Center, Ispra, Italy, Aprilie 2017; prezentare de tip poster.

[11] ***R.C. Popescu***, *R. Truşcă, B. Vasile, M. Straticiuc, A. Apostol, G. Voicu, E. Andronescu, D. Savu, A.M. Grumezescu*. "Doxorubicin- functionalized magnetite nanoparticles with anti-tumor applications: focus on electron microscopy investigations"CREMS, Sinaia, Romania, April 2017; prezentare de tip poster.

[12] ***R.C. Popescu***, *E. Andronescu, A.I. Apostol, M. Straticiuc, B.S. Vasile, A.M. Grumezescu, M.R. Veldwijk , D. Savu*. "Fabrication and testing of novel multifunctional nanosystems for chemo- and radio- sensitizing of tumor cells"RAD2017, Fifth International Conference on Radiation and Application in Various Fields of Research, Budva, Montenegro, Iunie 2017; prezentare orală.

[13] ***R.C. Popescu***, "Fabrication and testing of novel multifunctional nanosystems for chemo- and radio- sensitizing of tumor cells"Sesiunea de comunicări ştiinţifice a tinerilor cercetători din IFIN-HH, 19-12 Decembrie 2016, Măgurele, România; prezentare orală.

[14] ***R.C. Popescu***, *A.I. Apostol, E. Andronescu, A.M. Grumezescu, D. Savu*. "Fabrication of functionalized magnetite nanoparticles with applications in drug delivery systems"12-th National Medical Physics and Biomedical Engineering Conference, NMPEC-2016, Sofia, Bulgaria, Noiembrie 2016; prezentare orală.

[15] ***R.C. Popescu***, *E. Andronescu, A.I. Apostol, C. Mustaciosu, R. Truşcă, B. Vasile, G.D. Mogoşanu, L. Mogoanţă, A.M. Grumezescu, D. Savu*. "Doxorubicin functionalized magnetite nanoparticles- enhancers in radiotherapy"Symposium of the Young Chemical Engineers, SICHEM 2016, Politehnica University of Bucharest, Septembrie 2016, Bucureşti, România; prezentare orală.

Research grants:

[1] "Improvement of the tumor response to radiotherapy (including ion beam therapy) by nanoparticles", Bundesministerum fur Bildung, Wissenschaft und Forschung (BMBWF) prin Austrian Agency for International Cooperation in Education and Research (OeaD), Ernst Mach Grant-worldwide nr. ICM-2018-10056, at Medical University of Vienna, between January 2019- February 2019.

[2] "Development and testing of novel multifunctional nanosystems for chemo- and radio-sensitizing of tumor cells", Agenția de finanțare Deutscher Akademischer Austauschdienst (DAAD), DAAD Research Grants for Doctoral Candidates and Young Academics and Scientists nr. 57299291, at Heidelberg University, Medical Faculty of Mannheim, between October 2017- June 2018.

V. References

[1]. *** Amag Pharmaceuticals. http://www.amagpharma.com/our-products/ (accessed on November 19th 2019).

[2]. *** MagForce- Fighting Cancer with Nanomedicine. http://www.magforce.de/en/home.html (accessed on October 7th 2019).

[3]. *** Feraheme- Ferumoxytol Injection. https://www.feraheme.com (accessed on November 19th 2019).

[4]. *Q. Tian, W. Ning, W. Wang, X. Yuan, Z. Bai.* "Synthesis of size-controllable Fe_3O_4 magnetic submicroparticles and its biocompatible evaluation *in vitro*" in J. Cent. South Univ., **vol. 23**, 2016, pp. 2784–2791.

[5]. *K. Gu, R.H. Fang, M.J. Sailor, J.H. Park.* "*In vivo* clearance and toxicity of monodisperse iron oxide nanocrystals" in ACS Nano, **vol. 6**, 2012, pp. 4947–4954.

[6]. *Q. Li, C.W. Kartikowati, S. Horie, T. Ogi, T. Iwaki, K. Okuyama.* "Correlation between particle size/domain structure and magnetic properties of highly crystalline Fe_3O_4 nanoparticles" in Sci. Rep., **vol. 7**, 2017, 9894.

[7]. *W. Wu, Q. He, C. Jiang.* "Magnetic Iron Oxide Nanoparticles: Synthesis and Surface Functionalization Strategies" in Nanoscale Res. Lett., **vol. 3**, 2008, pp. 397–415.

[8]. *R.C. Popescu, E. Andronescu, B. Vasile.* "Recent Advances in Magnetite Nanoparticle Functionalization for Nanomedicine." in Nanomaterials, **vol. 9**, nr. 12, 2019, 1791.

[9]. *A. Radon, A. Drygała, L. Hawełek, D. Łukowiec*. "Structure and optical properties of Fe_3O_4 nanoparticles synthesized by co-precipitation method with different organic modifiers." Mater. Charact., **vol. 131**, 2017, pp. 148–156.

[10]. *M. Anbarasu, M. Anandan, E. Chinnasamy, V. Gopinath, K. Balamurugan*. "Synthesis and characterization of polyethylene glycol (PEG) coated Fe_3O_4 nanoparticles by chemical co-precipitation method for biomedical applications." Spectrochim. Acta Mol. Biomol. Spectrosc., **vol. 135**, 2015, pp. 536–539.

[11]. *N.L. Chaves, I. Estrela-Lopis, J. Böttner, C.A. Lopes, B.C. Guido, A.R. de Sousa, S.N. Báo*. "Exploring cellular uptake of iron oxide nanoparticles associated with rhodium citrate in breast cancer cells." Int J Nanomed, **vol. 12**, 2017, pp. 5511-5523.

[12]. *Q. Feng, Y. Liu, J. Huang, K. Chen, J. Huang, K. Xiao*. "Uptake, distribution, clearance, and toxicity of iron oxide nanoparticles with different sizes and coatings." Sci Rep, **vol. 8**, 2018, 2082.

[13]. *K. Li, X. Zhao, B.K. Hammer, S. Du, Y. Chen*. "Nanoparticles Inhibit DNA Replication by Binding to DNA: Modeling and Experimental Validation." in ACS Nano, **vol. 7**, 2013, pp. 9664–9674.

[14]. *R. Generalov, W.B. Kuan, W. Chen, S. Kristensen, P. Juzenas*. "Radiosensitizing effect of zinc oxide and silica nanocomposites on cancer cells." in Colloids Surf. B Biointerfaces, **vol. 129**, 2015, pp. 79–86.

[15]. *S. Her, D.A. Jaffray, C. Allen*. "Gold nanoparticles for applications in cancer radiotherapy: Mechanisms and recent advancements." in Adv. Drug Deliv. Rev., **vol. 109**, 2017, pp. 84–101.

[16]. *M. Roser, H. Ritchie*. "Cancer" https://ourworldindata.org/cancer, 2015.

[17]. *** World Health Organisation. Cancer https://www.who.int/news-room/fact-sheets/detail/cancer, 2018.
[18]. *** Medichub.Ritmul lumii medicale. Romania in Global Cancer Statistics 2018. https://www.medichub.ro/reviste/oncolog-hematolog-ro/romania-in-global-cancer-statistics-2018-id-2019-cmsid-68, 2018
[19]. *R. Massart.* "Preparation of aqueous magnetic liquids in alkaline and acidic media" in IEEE Trans. Magn., **vol. 17**, 1981, pp. 1247–1248.
[20]. ***R.C. Popescu***, *E. Andronescu, B.S. Vasile, R. Trusca, A. Boldeiu, L. Mogoanta, G.D. Mogosanu, M. Temelie, M. Radu, A.M. Grumezescu, D. Savu*. "Fabrication and Cytotoxicity of Gemcitabine-Functionalized Magnetite Nanoparticles." Molecules, **vol. 22**, 2017, 1080.
[21]. *B. Li, H. Cao, J. Shao, M. Qu*. "Enhanced anode performances of the Fe_3O_4-Carbon-rGO three dimensional composite in lithium ion batteries." Chem. Commun., **Vol. 47**, 2011, pp. 10374–10376.
[22]. *S. Ahlberg, A. Antonopulos, J. Diendorf, R. Dringen, M. Epple, R. Flöck, W. Goedecke, C. Graf, N. Haberl, J. Helmlinger*. "PVP-Coated, negatively charged silver nanoparticles: A multi-center study of their physicochemical characteristics, cell culture and in vivo experiments." Beilstein. J. Nanotechnol., **vol. 5**, 2014, pp. 1944–1965.
[23]. *** The RRUFF Project The Database. Magnetite R061111. http://rruff.info/magnetite/R061111 (Accessed on 22.07.2020).
[24]. ***R.C. Popescu***, *M. Straticiuc, C. Mustaciosu, M. Temelie, R. Trusca, B.S. Vasile, A. Boldeiu, D. Mirea, R.F. Andrei, C. Cenusa, L. Mogoanta, G.D. Mogosanu, E. Andronescu, M. Radu, M.R. Veldwijk, D.I. Savu*, "Enhanced Internalization of Nanoparticles Following Ionizing Radiation Leads to Mitotic Catastrophe in MG-63 Human Osteosarcoma Cells." Int J. Molec. Sci., 2020, **vol. 21**, nr. 19, 7220.
[25]. ***R.C. Popescu***, *D.I. Savu, A.D. Olarescu, O. Gherasim, S. Banita, M. Straticiuc, D. Mirea, R.F. Andrei, R. Trusca, B.S. Vasile, G. Socol, E. Andronescu*. "In vitro magnetic targeted delivery of doxorubicin using iron oxide nanoparticles leads to enhanced cell death in glioblastoma." U.P.B. Sci. Bull, Series B, **accepted for publication**, 2020.
[26]. ***R.C. Popescu***, *D. Savu, I. Dorobantu, B.S. Vasile, H. Hosser, A. Boldeiu, M. Temelie, M. Straticiuc, D.A. Iancu, E. Andronescu, F. Wenz, F.A. Giordano, C. Herskind, M.R. Veldwijk*. "Efficient uptake and retention of iron oxide-based nanoparticles in HeLa cells leads to an effective intracellular delivery of doxorubicin." Sci Rep, **vol. 10**, 2020, 10530.
[27]. *E. Mini, S. Nobili, B. Caciagli, I. Landini, T. Mazzei*. "Cellular pharmacology of gemcitabine." Ann. Oncol., **vol. 17**, 2006, pp. v7–v12.
[28]. *S. Sabella, R.P. Carney, V. Brunetti, M.A. Malvindi, N. Al-Juffali, G. Vecchio, S.M. Janes, O.M. Bakr, R. Cingolani, F. Stellacci*. "A general mechanism for intracellular toxicity of metal-containing nanoparticles." Nanoscale, **vol. 6**, 2014, pp. 7052–7061.
[29]. *A.R. Munoz-Duarte, N.S. Castrejon-Jimenez, S.L. Bltierra-Uribe, S.J. Perez-Rangel, N. Carapia-Minero, J.I. Castaneda-Sanchez, J. Luna-Herrera, R. Lopez-Santiago, A.V. Rodriguez-Tovar, B.E. Garcia-Perez*. "Candida glabrata survives and replicate in human osteoblasts." Pathogens and Disease, vol. 74, nr. 4, 2016, ftw030.